(4)

Fundamental and Practical Studies of Metal Contacts on Mercury Zinc Telluride

Sponsored by

The Defense Advanced Research Projects Agency (DoD)

Administered through the

The Office of Naval Research

ARPA Order: 5674 FRC H414 dated 01/86 August 22

Contract No. N00014-86-K-0854

Annual October 1, 1986 to December 31, 1987

Principal Investigator: W. E. Spicer
Stanford Electronics Laboratories
Stanford University
Stanford, CA 94305-4055
(415) 723-4643

Annual Technical Report
DARPA Contract No. N00014-86-K-0854
January 1 - December 31, 1987

G. P. Carey, A. K. Wahi, D. J. Friedman, I. Lindau, and W. E. Spicer
Stanford Electronics Lab, Stanford University, Stanford, CA 94305

Section I - Introduction

Metal/HgCdTe interfaces generally are characterized by profound intermixing of the semiconductor components and severe Hg loss upon metal deposition. The resulting disruption and interfacial instabilities at the interface prove deletorious to device stability and performance. During this reporting period, we have initiated several experimental studies pertinent to a greater understanding of the role of the weak Hg-Te bonding during interface formation. The behavior of metal contacts on HgCdTe and HgZnTe has also been examined in a theoretical study, in order to gain fundamental insight into mechanisms of Fermi level movement in these alloys. In this report we describe in detail results of these studies.

Section II provides a basic framework from which to understand the electrical behavior of metallic contacts to HgCdTe and HgZnTe. With knowlegde of the Fermi level pinning position in the binaries CdTe and ZnTe, one can extrapolate through the range of alloy compositions to make predictions for the behavior of metallic contacts to the alloys. It is predicted that for HgCdTe of $x < 0.4$, the compositions generally of interest to the infrared imaging community, ohmic contacts are expected on n-type HgCdTe and Schottky barriers are expected on p-type HgCdTe for all metals. The same considerations can be applied to HgZnTe.

Section III presents the results of our study using low temperature to reduce intermixing at metal/HgCdTe interfaces. This approach allows simplification of the interface by inhibiting metal interdiffusion, chemical reactions, and Hg loss; and it permits isolation of the various mechanisms that produce Fermi level movement at these interfaces, allowing us to separate effects due to interface disruption that occurs upon metal deposition.

In Section IV we present the results of a study of noble metal/CdTe interface formation. By studying interfaces with the binary CdTe, fundamental information relating to the additional role of the weak Hg-bonding in the alloy HgCdTe can be obtained. In addition, the Fermi level pinning positions are obtained which allow prediction of metal contact behavior (Schottky or ohmic) on HgCdTe.

Section II-The Electrical Properties of Metallic Contacts on $Hg_{1-x}Cd_xTe$

I. Introduction and Terminology

Metal contacts on semiconductors play a key role in device fabrication and long term reliability. However, the basic understanding of such contacts is often lacking. The object of this paper is to provide a framework for such basic understanding for $Hg_{1-x}Cd_xTe$ (MCT).

For the purpose of this paper, it is useful to identify the key parameter for determining the electrical properties of metal contacts. This is, E_{fi}, the position of the Fermi level in the semiconductor at the metal/semiconductor interface (see Figure 1). We will adopt the convention that E_{fi} is measured from the valence band maximum (VBM). E_{fi} is usually the same independent of the doping of the semiconductor. If it lies in the conduction band (valence band), an ohmic contact is formed on n-type (p-type) semiconductors. Conversely, a rectifying contact will be formed on p-type (n-type) semiconductors. If, as is often the case, E_{fi} falls in the band gap, rectifying contacts (Schottky barriers) are formed on both n- and p-type semiconductors. We would like to define the terminology for ohmic contacts which will be used in this paper. There are two types of ohmic contacts (Fig. 2). In one type E_{fi} is at or above the conduction band minimum (CBM) for n-type material (or at or below the VBM for p-type). This is an intrinsic ohmic contact. For brevity we will refer to this as ohmic throughout most of this paper, and the case for n-type is shown in Fig. 2a. A second type of ohmic contact (Fig. 2b) is obtained if E_{fi} lies in the bandgap by doping the interfacial region so highly that electrons can tunnel through the barrier. This is an extrinsic ohmic contact. We will not consider this type of contact until Section IV.

Our approach in providing a framework of understanding for metal contacts on MCT is to use the knowledge of Schottky barrier pinning on semiconductors to predict the characteristics to be expected for MCT. Three different models of Schottky barrier pinning will be used; however, as will be seen, all give similar predictions. Because E_{fi} plays such an important role in determining the electric properties of metal contacts, we will concentrate on this parameter. One of the characteristics of E_{fi} is that it does not vary much from one metal to another. Due to this, we will treat E_{fi} as metal independent for most of this paper. However, toward the end we will consider possible variations in E_{fi} due to the specific metal used.

To gain insight into the $Hg_{1-x}Cd_xTe$ system, it is interesting to examine the $In_{1-x}Ga_xAs$ alloy system for GaAs since E_{fi} lies near mid gap (as in Fig. 3) so that rectification is obtained on both n- and p-type GaAs (intrinsic Schottky barriers). Ohmic contacts are believed to be made by heavily doping the interface region so that carriers can tunnel through the barrier forming a low resistance extrinsic ohmic contact (Fig. 2b). As increasing In is alloyed into GaAs, the CBM moves toward the VBM (*i.e.* the band gap decreases) and E_{fi} moves into the conduction band. (see for example Ref. 1). Thus for $In_{1-x}Ga_xAs$ of $x < 0.5$ one would have an intrinsic ohmic contact on n-type material (Fig. 2a) but intrinsic Schottky barriers for p-type for all values of composition. As will be developed in this paper, we find a very similar situation for MCT.

II. Location of E_{fi} (Schottky Barrier Height) for CdTe

The first step here is to use experimental data to place a limit on E_{fi} for CdTe. Two methods have been used to locate E_{fi}. One is the by measuring electrical properties [2]. The other is by photoemission spectroscopy (PES) measurements [3]. Careful measurements on GaAs and InP indicate that these two methods usually give E_{fi} values within 0.1 eV of each other [4]. The electrical measurements usually give a Schottky barrier height for either n-type, $\varphi_{b,n}$, or p-type material, $\varphi_{b,p}$. Equation (1) and (2) indicate the relationship between E_{fi} and these barrier heights:

$$E_{fi} = E_g - \varphi_{b,n} \quad (1)$$

$$E_{fi} = \varphi_{b,p} \quad (2)$$

where E_g is the band gap.

Friedman *et al.* [5] has recently reviewed the literature for the noble metals, Cu, Ag, and Au, on CdTe. The results are presented in Table 1. Note that this table contains results from both PES and electrical measurements. Note that of the 21 values of E_{fi} given in Table 1 and this text, only four fall below 0.75 eV and only one of these by more than 0.1 eV.

Sze[6] also provides values of E_{fi} from electrical measurements for two non-noble metals: 0.8 for Al and 0.8 for Pt. Again the value lies above 0.75 eV.

For the purpose of the framework being built here, it is only necessary to provide a lower limit on E_{fi}. We will place this at 0.75 eV. Thus 0.75 eV appears to be a conservative lower limit for E_{fi} and this limit will be used throughout this text.

III. Prediction of E_{fi} for $Hg_{1-x}Cd_xTe$

A. Introduction

Following the approach outlined in the previous section, we have set a lower limit of 0.75 eV on E_{fi} for CdTe. We will now use three models of Schottky barrier pinning on semiconductors (*e.g.* see Flores and Tejedor [7]) to extrapolate from CdTe to $Hg_{1-x}Cd_xTe$. Two of the models of Schottky barrier pinning, the defect model of Spicer *et al.* [3,8] and the metal induced gap state (MIGS) model will be examined first. The third model, the Effective Work Function Model of Freeouf and Woodall [9] will be examined separately in section IIIE.

The defect model is more formally known as the Unified Defect Model since it is applicable to insulators and other non-metals as well as metals. In this model, the position of E_{fi} is due to native defects produced by the perturbation of the semiconductor by the deposition of the metal or other overlayer. Recently, it has been suggested that for GaAs the key defect is an As antisite, *i.e.* a As on a Ga lattice site. Based on this an Advanced Unified Defect Model has been proposed [8] which seems able to explain a wide variety of data.

Heine [10] first suggested the metal induced density of states model which is now known as the MIGS model. Here the position of E_{fi} is believed to be set by states induced in the semiconductor at the metal/semiconductor interface due to tunnelling of electrons from the metal into the semiconductor. This model has been advanced by several groups [7]. We will make particular use of the work of Tersoff [11] since using Tersoff's work allows one to extrapolate from CdTe to $Hg_{1-x}Cd_xTe$.

In order to understand the extrapolations for both the defect and metal induced gap states (MIGS) models, it is important to understand the relationship between these extrapolations and the band structure of CdTe and $Hg_{1-x}Cd_xTe$. Both the energy levels of the defects and the E_{fi} position determined by the MIGS are strongly tied to the band structure. As one decreases the value of x,

(*i.e.* increases the Hg content) in the $Hg_{1-x}Cd_xTe$ alloy, the CBM, which is at the Γ point in the Brillouin zone, decreases faster than other parts of the conduction band and the valence band is only slightly affected [11]. The band gap changes faster than do other band structure features (see Figure 4). The net result of this, as we will see in the next two sections, is that the band gap decreases faster than E_{fi}, *i.e.* as the CBM moves toward the VBM, E_{fi} moves toward the VBM but more slowly than the CBM. As a result, the CBM crosses E_{fi} for either model near x = 0.5. For sufficiently low x, E_{fi} will lie in the conduction band. This will have profound consequences for the electrical behavior of metal contacts on MCT.

Having set a lower limit for E_{fi} for CdTe we will use results from these models to extrapolate E_{fi} as a function composition (x) in $Hg_{1-x}CdxTe$.

B. E_{fi} as a Function of Composition Using the Defect Model

Assuming that E_{fi} is set by defects, it is necessary to have a means of extrapolating the key defect level from CdTe to $Hg_{1-x}Cd_xTe$. One theoretical work for doing this is provided by the work of Tobayoshi, Sankey, and Dow [12] which gives the change in energy level due to change in variation in $Hg_{1-x}Cd_xTe$ composition for a wide variety of impurities and defects in MCT. Taking our lower limit of E_{fi} for CdTe 0.75 eV and extrapolating using the results of Ref. 12, we obtain the diagonal line labeled E_{fi} in Fig. 5. This indicates the lower limit of E_{fi} as a function of x. The second diagonal line labeled "CBM" in Fig. 5 gives the CBM as a function of x, and we see that E_{fi} will lie in the conduction band for $x < 0.4$ or $Eg < 0.46$ eV and

$$E_{fi} = 0.25 + 0.5x \qquad (3)$$

Thus, one would expect ohmic contacts on n-type for x and E_g of $Hg_{1-x}Cd_xTe$ less than the indicated values. Conversely, one would expect rectifying contacts for metals on p-type materials of all composition.

Included in the work of Ref. 12 is Te on a Cd site, *i.e.* a Te_{Cd} antisite defect. The calculated energy level in CdTe is about 0.95 eV. If we were to take E_{fi} equal to the defect energy level, we would obtain $E_{fi} = 0.95$ eV for CdTe. This is in the range of experimental values for E_{fi}

given in Table III-2 (in section III of this report) and makes the Te antisite an interesting candidate for the defect which plays a key role in determining E_{fi} [12].

Zunger and co-workers [13] have examined the movement of the energy levels of deep, antibonding, cation site impurities in alloys and find that, once an absolute energy scale is found, that these energy levels lie at a constant energy on that scale independent of alloy composition. Moreover, the VBM moves in going through the alloy from one binary to the other by an amount just equal to the VBM offset between the two materials. Since the best value for the VBM offset of MCT with respect to CdTe is 0.35 eV (*i.e.* the VBM of MCT lies 0.35 eV above that of CdTe), the impurity level would move linearly downward by 0.35 eV in going from CdTe to MCT as shown in Figure 5. If we assume that the defect levels behave as these impurities, then we would place the lower limit of E_{fi} on that line. Thus, we find that E_{fi} moves into the conduction band for $x < 0.5$ ($E_g < 0.65$).

C. Extrapolation of E_{fi} Using the MIGS Model

Tersoff [11,14] has defined a quantity E_B which is the position where the MIGS mechanism will place E_{fi}; thus, by definition $E_B = E_{fi}$. Terscff has calculated values of E_B of 0.85 eV for CdTe and 0.34 for HgTe. The CdTe value lies just above our limit of 0.75 eV. According to Tersoff's theory, the difference in E_B for any two semiconductors gives the valence band discontinuity when they are brought together to form a heterojunction. By comparing Tersoff's predicted heterojunction offset to experiment [15,16], we can empirically evaluate his approach. Using the value of E_B given above, he predicts a value of 0.51 ± 0.2 eV in reasonable agreement with the experimental values of 0.35 ± 0.05 eV. Tersoff states that E_B for alloys can be estimated by linear interpolation. In keeping with our approach of using experimental values, we will take E_{fi} ($x = 0$) = 0.35 eV and $E_{fi}(x = 1)$ = 0.75 eV. This gives results within the error limits given by Tersoff. Note, however, that they lie near the lower limit of his error bars; thus, the values calculated should be considered to be close to a lower limit. Using these values, we find

$$E_{fi}(x) = 0.35 + 0.4x \qquad (4)$$

for the position of E_{fi} as a function of composition. Equation 4 is plotted on Figure 5. Note that it is nearly identical to the value obtained from the impurity level work of Zunger and co-workers in the preceding section. Thus one finds that E_{fi} lies in the conduction band for $x < 0.5$. Thus for $E_g < .65$ eV, one would have an ohmic contact on n-type material

D. The Effective Work Function Model

In the Effective Work Function (EWF) model of Freeouf and Woodall [9], E_{fi} is set via a Schottky mechanism [2] by the work function difference between a solid made up of the anion of the semiconductor and of the semiconductor. Although PES has not given evidence of such a Te layer at the interface, we will examine the prediction of this model for completeness. In the effective work function model, it is assumed that the Schottky barrier height is set by the classic Schottky-Mott theory [1]. In that theory, the barrier height on n-type material, $\varphi_{b,n}$, is given by:

$$\varphi_{b,n} = \varphi - E_a \qquad (5)$$

where φ is the work function of the metal (taken to be that of Te in this development) and E_a is the electron affinity of the semiconductor. Since we are interested in E_{fi} rather than $\varphi_{b,n}$, we can use equation (5) to write equation (1) in the form

$$E_{fi} = (E_g + E_a) - \varphi \qquad (6)$$

$(E_g + E_a)$ is just the energy difference from the valence band to the vacuum level, *i.e.* the energy needed to take a electron from the VBM to vacuum in front of the semiconductor. We take $E_o = E_g + E_a$, where E_o is the threshold for photoemission from the valence band

and $$E_{fi} = E_o - \varphi. \qquad (7)$$

Since φ is for Te and this is fixed, it is only E_o which will vary as composition is changed in $Hg_{1-x}Cd_xTe$. Using this model, we assume that E_{fi} for CdTe is set by equation (7) and that $\Delta E_{fi} = \Delta E_o$ as composition is varied.

Casselman *et al.* [17] provide a tabulation of values for $Hg_{1-x}Cd_xTe$. To this we would like to add recent values obtained by Shih [18]: (1) HgTe, $E_o = 5.2 \pm 0.15$, (2) $Hg_{0.7}Cd_{0.3}Te$, $E_o = 5.65 \pm 0.15$; and (3) CdTe, $E_o = 6.0 \pm 0.15$. Shevick *et al.* [17] obtained a decrease in E_o of 0.3 eV in going from CdTe to HgTe, whereas Casselman *et al.* found a decrease of 0.2 eV in

going to x = 0.39 material with a more rapid drop as x became smaller. Note that Shih found a drop of 0.35 eV in going from CdTe to x = 0.3 MCT. Making use of these results to obtain a lower limit on E_{fi} we take a 0.3 eV drop in going from CdTe to x = 0.4 eV material, we get a value for E_{fi} of 0.45 eV at x = 0.4 which compares with a bandgap of 0.46 eV at that composition. Thus, once again E_{fi} will move into the conduction band for x < 0.4 eV.

E. Summary

Each of these methods gives the same general result - ohmic contacts on n-type material for x less than a certain value and rectification for all p-type MCT. In Table 2, we indicate the values of x and E_g at which the contacts on n-type material would become ohmic. Note that these are lower limits since 0.75 eV is taken as a lower limit of E_{fi}. Thus if the E_{fi} on CdTe were larger, the value of x at which E_{fi} reaches the CBM would be corresponding larger. Note also that contacts on semiconductors tend to appear ohmic before the barrier height goes completely to zero. This again makes our estimate here a lower limit. Thus, it appears to be a conservative statement of the present results to conclude that intrinsically ohmic contacts would be expected on n-type MCT for x < 0.4. In contrast Schottky barriers would be expected on p-type MCT semiconductors independent of composition.

IV. Implications for Practical Metal Contacts

In the preceding section we have attempted to use our present knowledge of metal contacts on semiconductors to predict the behavior on $Hg_{1-x}Cd_xTe$ behavior. The results indicate that, for x values in the range of interest for the infrared imaging community, *i.e.* less than about 0.4, one would have ohmic contacts on n-type and Schottky values on p-type material. The authors of this paper have been unsuccessful in obtaining published data on the electrical properties of metal contacts on MCT. Hopefully, the recent fundamental work on this subject, *e.i.* the other metal/MCT papers in this volume are examples of that work, will stimulate future publications of the electrical properties of metal contacts on MCT. However, it is important to note that most focal plane arrays and other devices put into service to date require only ohmic contacts on n-type MCT

and there does not seem to have been a serious problem in obtaining such contacts. This is in agreement with the analysis presented here, *i.e.* intrinsic ohmic on n-type. On the other hand, based on private discussions there seems to be much more difficulty in making ohmic contacts on p-type material. In fact there does not seem to be any established technology for doing this. Again this is as would be expected from our analysis In this section we will address the problem of forming ohmic contacts on p-type MCT.

There seems to be no MCT devices which depend on Schottky barriers. However, the experience with ohmic contacts on n-type material would indicate difficulty in forming Schottky barriers on n-type material. We will address this problem in this section. In contrast, our analysis would indicate that Schottky barriers would be easy to form on p-type material.

Let us first examine the situation with regard to ohmic contacts on p-type material. Fig. 2b shows an extrinsic ohmic contact on n-type MCT. Up to this point we have concentrated on intrinsic ohmic contacts on MCT (shown in Fig. 2a); however, when one does not have an intrinsic ohmic contact (as is the case for Si and GaAs), one must resort to extrinsic ohmic contacts. In the case shown in Fig.2b, this is obtained by doping the region close to the contact so strongly n-type that the depletion width becomes small enough so that electrons can easily tunnel through it. Usually doping of $10^{19}/cm^3$ or above is necessary to give excellent ohmic contacts. For p-type material the situation would be the same except that high p-type doping would be necessary. This would be the most straight forward way of making an ohmic contact on p-type MCT.

Some indication of a doping by the metal forming the contact has been presented by Friedman et al. [19]. As they report, using PES it is found that for three metals known to dope MCT p-type (Cu, Ag, and Au) E_{fi} moves about 0.1 eV toward the VBM due to deposition of the metal. In contrast, two metals, Al and In, which dope MCT n-type, E_{fi} moved into the conduction band by 0.4 or 0.5 eV. These data suggest that an appreciable number of the metal atoms move into and strongly dope the MCT. This is not surprising since all researchers who have used PES

to study metal contact formation on MCT have found the surface to be torn up by deposition of the metal much more strongly than semiconductors such as GaAs or Si [19-21].

The fact that E_{fi} is seen to move means that a high degree of doping has been achieved. Note that the situation as shown in Fig. 2b for obtaining an ohmic contact does not require movement of E_{fi}. The fact that E_{fi} is seen to move at the surface of p–type MCT by PES indicates that the doping level is quite high. This suggests that doping by the properly chosen deposited metals might provide ohmic contacts on p-type material. However, two types of warnings should be made. First, most PES studies were made on atomically clean surfaces; whereas, practical contacts may more commonly be made on MCT surfaces covered with various foreign films, for example, oxides. The presence of these films could retard the interactions between the deposited metal and the MCT and, thus, the doping by the metal. The second warning related to long term stability. If the ohmic contact on MCT depends on the relatively uncontrolled process described above, one has to worry whether the situation is time stable or whether there is danger that the system will relax, adversely affecting the desired contact properties. More work is needed in both these areas. The work of Davis *et al.* [20] indicates how PES can be used to study the effect of surface preparation on the interaction between the deposited metal and MCT. Raisanen *et al.* [21] have demonstrated how metal:MCT chemistry and multi-metal depositions can be used to control interface diffusion and reactions. Likewise, the work of Carey *et al.* [22] indicates one approach of using temperature to control the disruption of the MCT and to study long term interface stability. More work of this type using PES is necessary. Even more pressing are electrical measurements which can be correlated with the PES and practical needs. Both electrical measurements and PES work should be brought to bear in order to devote a more viable contact technology.

It should be recognized, that ohmic contacts on GaAs and Si are thought to be formed by heavy doping by an element other than the deposited metal. In GaAs, Au/Ge/Ni contacts are most common on n-type material. It is thought that the Ge diffuses into the interface region during post deposition annealing step. In Si shallow ion implantations are often used to reduce the contact resistance. These types of technologies are also possibilities for MCT.

Normally Schottky barrier heights (and thus E_{fi}) are found to be modestly effected by the electronegativity of the metal applied [2,4]. As the electronegativity increases, E_{fi} moves toward the VBM. For GaAs, changes of as much as 0.2 or 0.3 of an eV are found [2]. However, the PES results on MCT gives no clear evidence of such a shift upon deposition of Pt and Pd [19]. This may be because the normal E_{fi} position lies sufficiently above the CBM so that the electronegativity effect is not important. However, the available data is only suggestive not conclusive. Thus it is important that the effect of the electronegativity of the metal on the contact properties also should be studied.

If Schottky barriers on n-type MCT are desired, one approach would be to heavily dope the interface p-type. This can provide a structure somewhere between a Schottky barrier and a p-n junction which has Schottky barrier-like behavior.

It would be inappropriate to end this section without re-emphasizing potential materials stability problems of metal/MCT contacts. MCT is a difficult material because of the ease with which it can be damaged. Direct evidence of this in the present context is provided by the PES studies [19-22], which directly show disruption of MCT due to metal deposition. Because the delicate nature of MCT, time and temperature stability may be a problem with MCT contacts. This will be particularly true where extrinsic (high doping) contacts must be made. Examples are such as the p-type ohmic or n-type Schottky barrier contacts discussed above. Since, historically, contacts and metallization are often one of the key factors in limiting yield in monolithic semiconductor production, it is important that MCT effects be well understood and controlled.

V. Conclusions

The various models for Schottky barrier formation, all indicate that metal contacts on MCT will be intrinsically ohmic on n-type and rectifying (Schottky barriers) on p-type MCT. This seems to be in agreement with much practical experience on MCT. However, there is a large need for more data in the published literature on the electrical characteristics of various metals on MCT particularly at the operating temperatures of the devices.

* Supported by DARPA and ONR under contract No. N00014-86-K-0854

Acknowledgement: Valuable discussions with T. Casselman, C. R. Helms, J. Murphy, G. Roberts, and C. K. Shih are gratefully acknowledged.

References

a) Stanford Ascherman Professor of Engineering

1. W. E. Spicer and S. J. Eglash in VLSI Electronics **10**, ed. by N. G. Einspruch and R. S. Bauer, Academic Press, N.Y., 1985.
2. E. H. Rhoderich, Metal-Semiconductor Contacts, Clarenden Press, Oxford, 1978.
3. W. E. Spicer, P. W. Chye, P. R. Skeath, C. Y. Su, and I. Lindau, J. Vac. Sci. and Technol. **16**, 1427 (1979); **17** 1019 (1980).
4. N. Newman, W. E. Spicer, T. Kendelewicz, and I. Lindau, J. Vac. Sci. and Technol. **B 4**, 931 (1986).
5. D. J. Friedman, I. Lindau, and W. E. Spicer, to be published in Phys. Rev B.
6. S. M. Sze, Physics of Semiconductor Devices, 2nd ed., John Wiley and Sons, N. Y. 1981.
7. F. Flores and C. Tejidor, J. Phys. C., Solid State Phys **20**, 145 (1987).
8. W. E. Spicer, T. Kendelewicz, N. Newman, R. Cao, C. McCants, K. Miyano, I. Lindau, and E. Weber, to be published in J. Vac. Sci. Technol.
9. J. L. Freeouf and J. M Woodall, Appl. Phys. Lett. **39**, 727 (1981).
10. V. Heine, Phys. Rev. **138**, 1689 (1965).
11. J. Tersoff, Phys. Rev. B **32** 6968 (1985).
12. A. Kobayoshi, O. F. Shankey, and J. D. Dow, Phys. Rev. B **25**, 6367 (1982).
13. A. Zunger, "Electronic Structure of 3d Transition -Atomic Impurities" in Solid State Physics, **Vol. 39**, ed. by D. Turnbull and H. Ehrenreich, Academic Press, NY, 1987; M. J. Caldas, A. Fazzio, and A. Zunger, Appl Phys. Lett. **45**, 671 (1984); A. Zunger, Phys. Rev. Lett. **54**, 849 (1985).
14. J. Tersoff, Phys. Rev. Lett. **56**, 2755 (1986).
15. J-P Faurie, C. Hsu, and T. M. Duc, J. Vac. Sci. Technol. **A5**, 3074 (1987).
16. C. K. Shih and W. E. Spicer, Phys. Rev. Lett. **58**, 2594 (1987).

17. T. N. Casselman, A. Sher, J. Silberman, W. E. Spicer, and A. B. Chen, J. Vac. Sci. Technol. **A 1**, 1692 (1983).

18. C. K. Shih, private communication

19. D. J. Friedman, G. P. Carey, I. Lindau and W. E. Spicer, J. Vac. Sci. and Technol. **A5**, 3190 (1987) and references therein.

20. G. D. Davis, W. A. Beck, M. K. Kelly, D. Kilday, Y. W. Mo, N. Tache, and G. Margaritondo, J. Vac. Sci. and Technol. (in press); G. D. Davis, Vuoto Scienza e Technologia, **16**, 127 (1986) and references therein.

21. A. Raisanen, A. Wall, S. Chang, P. Philip, N. Troullier, A. Franciosi, and D. J. Peterson, J. Vac. Sci. Technol. (in press).

22. G. P Carey, D. J. Friedman, A. K. Wahi, C. K. Shih, and W. E. Spicer, J. Vac. Sci. Technol. (in press).

Predicted Value For x Which One Would Expect for Ohmic on n-type		
Model	x	E_g
Defect	0.4	0.46 eV
Defect	0.5	0.65 eV
MIGS	0.5	0.65 eV
EWF	~0.4	~0.46 eV

Table II. The lower limits on composition (x) and band gap (E_g) of $Hg_{1-x}Cd_xTe$ at which ohmic contacts would be expected as found by use of three models of Schottky barriers. The two values for the Defect Model were obtained using two different approaches as described in the text.

Figure 1

The relationship between the Fermi level at the interface, E_{fi}, and the intrinsic electrical properties. These diagrams show only the first few atomic layers of the semiconductor, so that no attempt is made to show the semiconductor band bending.

Figure 2

The meaning of ohmic contact as used in this paper. Figure 3a (upper panel) shows an intrinsic ohmic contact. This is the configuration which we will refer to as "ohmic" throughout this paper. An example of an extrinsic contact is shown in 3b. In section IV we will discuss the extrinsic ohmic contact.

Figure 3

Energy diagrams for n- and p-type semiconductor pinned near midgap. Here we show the semiconductor extending far enough from interface for the band bending to be apparent. The middle diagram of Figure 1 corresponds to the part of this diagram first at the interface.

Figure 4

Change in band structure of $Hg_{1-x}Cd_xTe$ in going from $x = 1$ to $x = 0.16$. Note that the conduction band maximum moves faster than other parts of the band structure. (band structures from Ref. 12)

Figure 5

Lower limit of the Fermi level position at the interface, E_{fi}, as a function of composition. Two models (MIGS and Defect) were used for this extrapolation. Near $x = 0.4$ E_{fi} moves into the conduction band providing intrinsic ohmic contacts on n-type material.

Use of E_{fi} to Define Intrinsic Properties of Contact

For $E_{fi} > E_g$:

Ohmic on n-type

Schottky on p-type

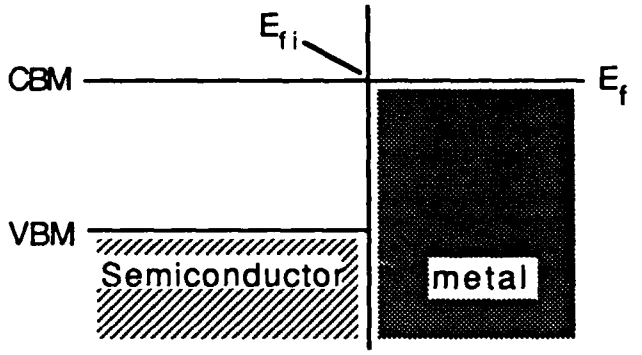

For $E_g > E_{fi} > 0$:

Schottky on both
n- and p-type

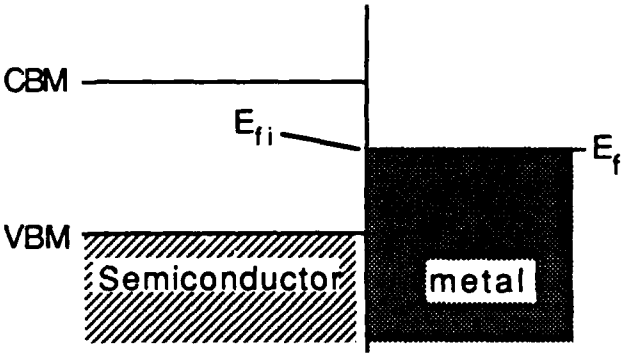

For $E_{fi} < 0$:

Ohmic on p-type

Schottky on n-type

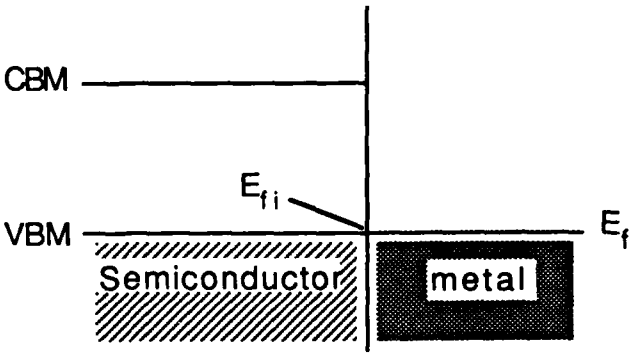

Figure 1

The 2 Types of Ohmic Contacts

a) Intrinsic Ohmic Contact

Ohmic Contact Independent of
Semiconductor Doping Near Interface

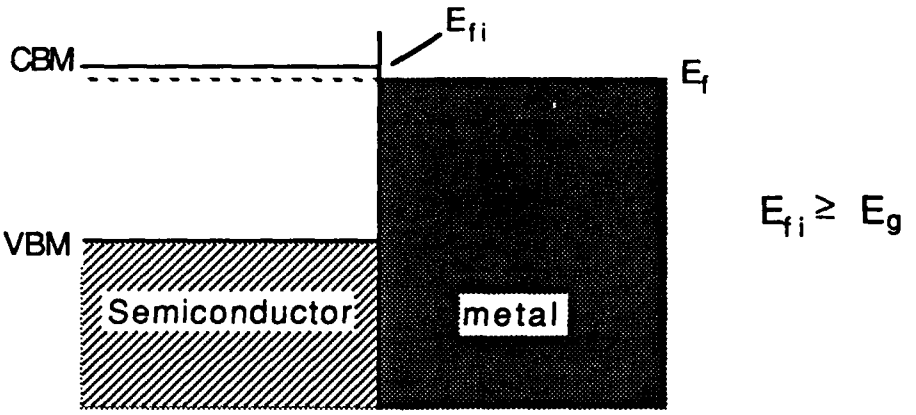

b) Extrinsic Ohmic Contact

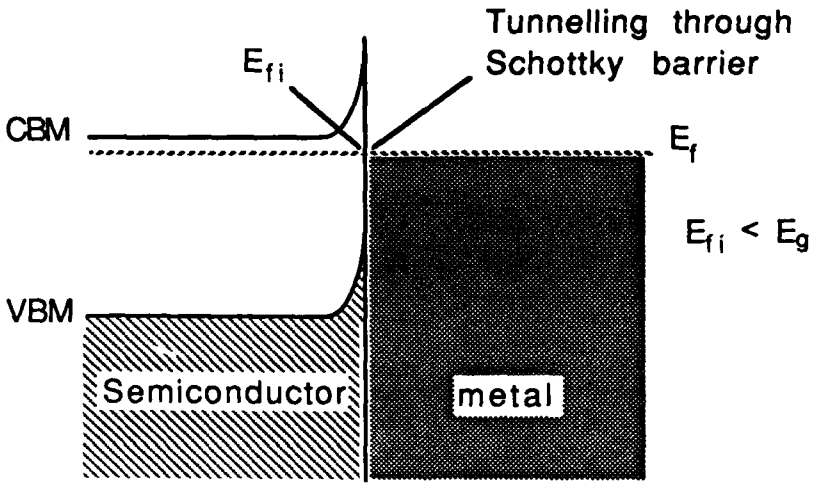

Figure 2

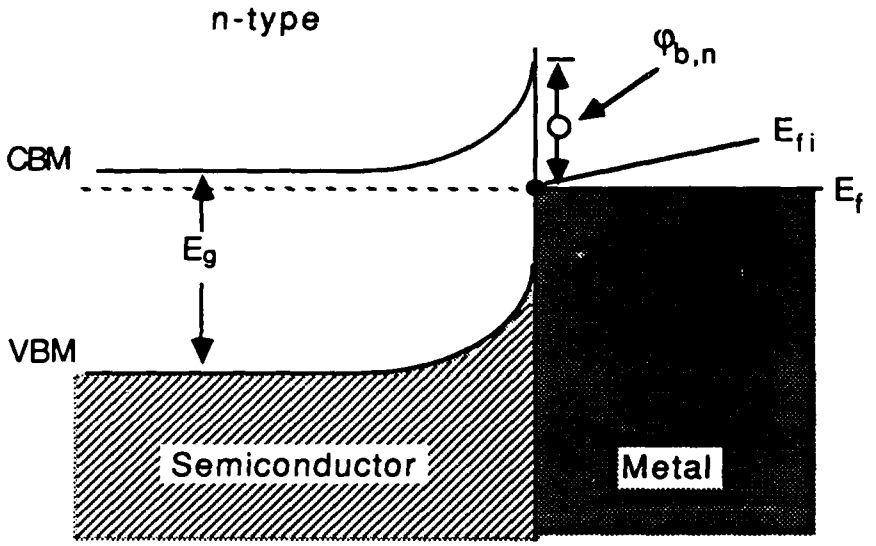

$$\varphi_{b,n} = E_g - E_{fi}$$

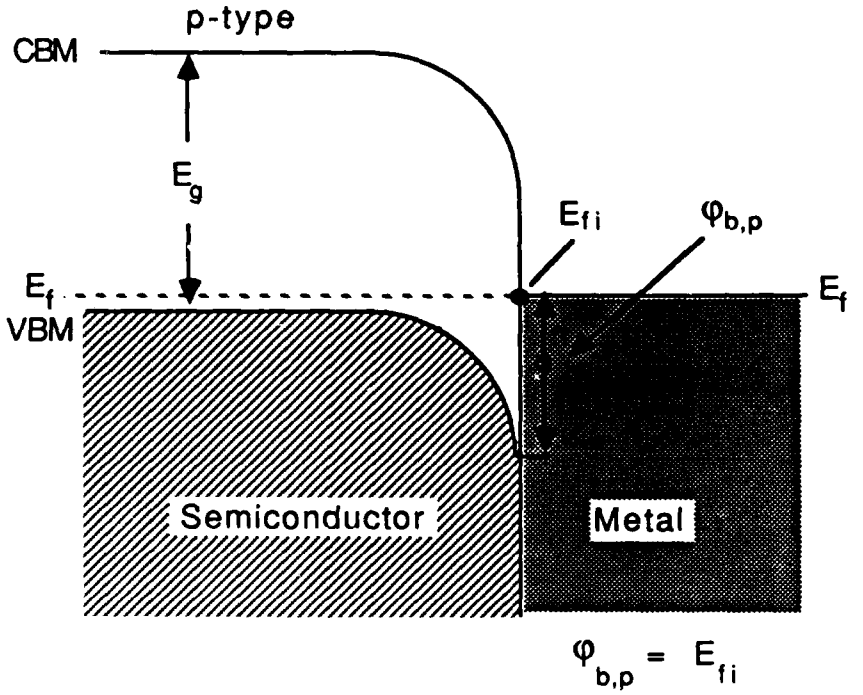

$$\varphi_{b,p} = E_{fi}$$

where: $\varphi_{b,n} \equiv$ Schottky Barrier Height on n-type

$\varphi_{b,p} \equiv$ Schottky Barrier Height on p-type

$E_{fi} \equiv$ position of Fermi level at interface (same on n- and p-type)

and $\varphi_{b,n} + \varphi_{b,p} = E_g$

Figure 3

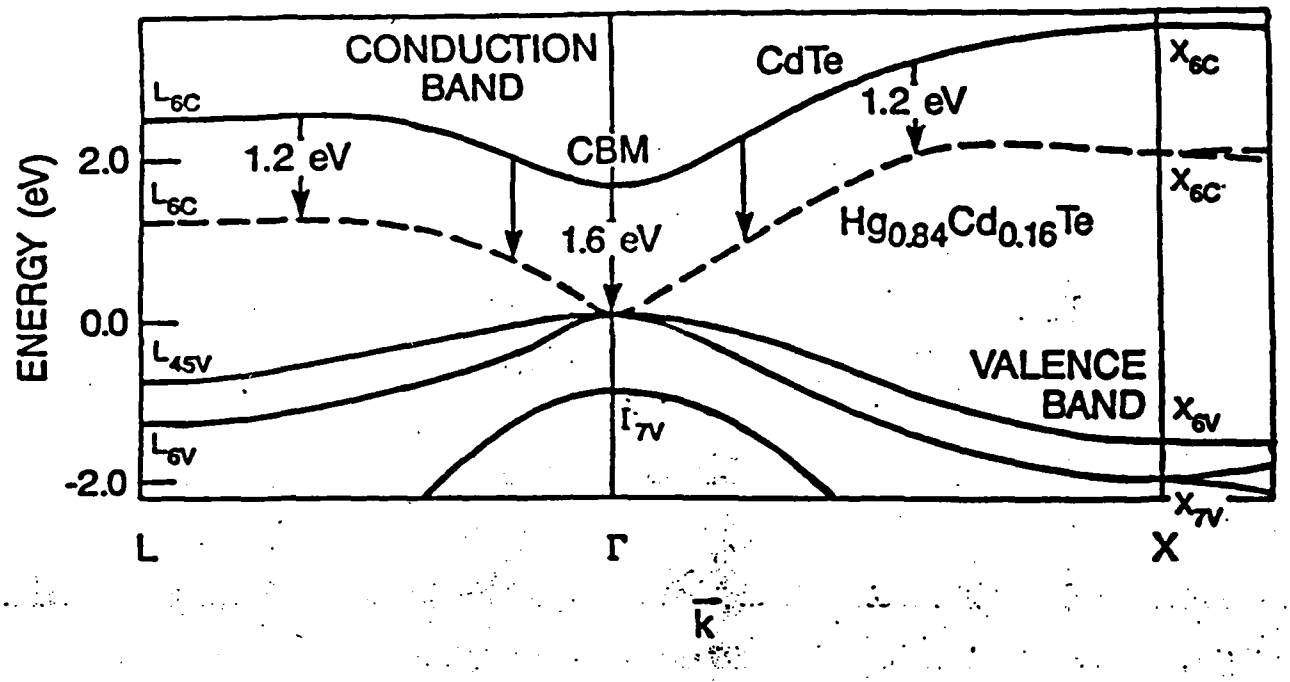
CONDUCTION BAND
CdTe
X_{6C}
L_{6C}
1.2 eV
1.2 eV
CBM
2.0
L_{6C}
X_{6C}
1.6 eV
$Hg_{0.84}Cd_{0.16}Te$
ENERGY (eV)
0.0
L_{45V}
VALENCE BAND
X_{6V}
Γ_{7V}
L_{6V}
-2.0
X_{7V}
L
Γ
X
k

Figure 4

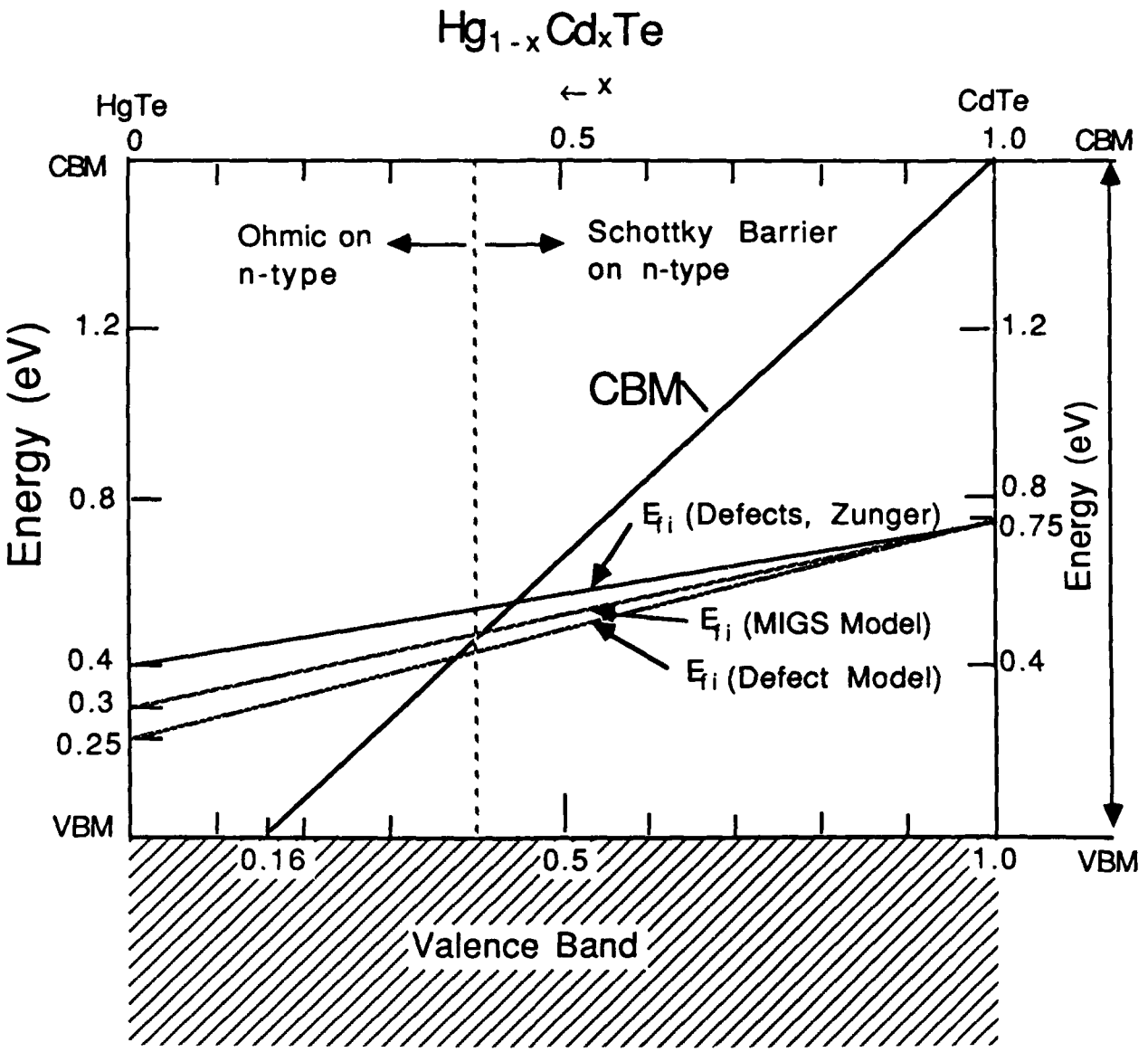
Hg1 - x Cdx Te
← x
HgTe
0
0.5
CdTe
1.0
CBM
CBM
Ohmic on
n-type
Schottky Barrier
on n-type
1.2
0.8
0.4
0.3
0.25
VBM
Energy (eV)
CBM
Efi (Defects, Zunger)
Efi (MIGS Model)
Efi (Defect Model)
1.2
0.8
0.75
0.4
Energy (eV)
0.16
0.5
1.0
VBM
Valence Band

Figure 5

Section III- Use of Low Temperature to Reduce Intermixing at Metal:HgCdTe Contacts

I. INTRODUCTION

Metal/HgCdTe interfaces formed at room temperature generally exhibit profound intermixing of the semiconductor and overlayer metal[1,2], to an extent far greater than for Si or GaAs. In addition, overlayers formed in ultrahigh-vacuum (UHV) under identical conditions on HgCdTe and CdTe show that the CdTe interfaces are much more abrupt than the corresponding HgCdTe interfaces[3,4], underlining the effect of the weak Hg-Te bond in the HgCdTe lattice.[5] The usual disruption at the interface upon overlayer formation and the concurrent loss of Hg in the near surface cause the interface to be very complex, both morphologically and electrically. Because of the complexity of these metal/HgCdTe contacts, it is difficult to model the defect levels present at the these interfaces and to gain insight into their role in the pinning of the surface Fermi level (E_f). In another paper of these proceedings, Spicer et al.[6] discusses in the framework of the current theories that address defect energy levels, how one can extrapolate from the measured defect energy levels in CdTe, which are well-tabulated, to those expected in the HgCdTe alloy.

Since metal contacts play an important role in the fabrication of semiconductor devices, recent efforts to reduce the Hg loss and consequent disruption of the HgCdTe lattice upon metal contact formation have been undertaken. Work performed by the Franciosi group[7,8] involves depositing rare-earth metals Sm and Yb, which form metallic phases having high Hg solubilities, to provide a possible kinetic barrier to Hg out-diffusion during subsequent contact formation. Thin kinetic diffusion barriers have also been investigated recently by Davis et al.[9] Since metal interdiffusion, chemical reactions and Hg loss should be inhibited in interfaces formed at lower temperatures, leading to a simplification of the interface, an experimental approach is followed in this study where Ag and Al are deposited in UHV ($p < 10^{-10}$ torr) onto atomically clean (110) $Hg_{0.61}Cd_{0.39}Te$ surfaces cooled to 170 K. These metals have vastly different telluride heats of formation ($\Delta H_f(Ag_2Te)$ = -8.6 and $\Delta H_f(Al_2Te_3)$ = -76.2 kcal/mole)[10], and result in very different

interface morphologies when deposited onto HgCdTe surfaces at the room temperature (RT). These RT interfaces have been discussed previously [11-13].

Since long term stability of metal contacts can also be problem[14], the stability of these interfaces formed at low temperatures (LT) is also of importance. As will be shown in this study, the LT formed Ag/HgCdTe interface exhibits instability upon annealing to RT, whereas the LT Al/HgCdTe interface appears stable when annealed at RT.

II. EXPERIMENT

A 10 mm long bar of single crystal $Hg_{0.61}Cd_{0.39}Te$ was transferred into a previously baked UHV chamber (base pressure < 10^{-10} torr) The crystal used in this study was grown at Santa Barbara Research Center. After allowing the crystal to cool down to 170 K, the sample was cleaved to reveal an atomically clean (110) face of cross-sectional area 5 x 5 mm. Although the crystal was grown bulk *p*-type, after cleaving the surface was observed to be inverted to *n*-type, which is commonly observed.[15] Sequential depositions of the metal were evaporated from a tungsten filament and the rate of evaporation was monitored with a quartz crystal microbalance. After each evaporation the surface was monitored with the surface sensitive techniques of photoemission spectroscopy (PES), using both x-ray photoemission spectroscopy (XPS) and ultra-violet photoemission spectroscopy (UPS), and low energy electron spectroscopy (LEED). The PES spectra was taken using a Mg Kα x-ray source ($h\nu$ = 1253.6 eV) for XPS and a He discharge lamp (He I and He II, $h\nu$ = 21.2 and 40.8 eV) for UPS. The photoelectrons were analyzed using a double-pass cylindrical-mirror analyzer with an integrating acceptance angle of 42.3 ± 6^{o}. For the taking of the LEED patterns, care was taken to minimize both the beam current (to less than 1 μA) and the exposure time, and no electron beam induced surface degradation effects were evident. The incremental metal coverages ranged from sub-monolayer (ML) at low coverages to several monolayers at higher coverages, where we define 1 ML to be the surface

density of atoms on the HgCdTe (110) face: 1 ML = 6.76 x 10^{14} atoms/ cm^2 which corresponds to 1.15 Å of metallic Ag or 1.12 Å of metallic Al.

III. RESULTS AND DISCUSSION

A. Morphology

The morphologies of the LT interfaces are significantly more abrupt and exhibit much less Hg loss at the surface than for the corresponding RT formed interfaces.[11-13] The following two sections present the photoemission and LEED results of the Ag/HgCdTe and Al/HgCdTe interfaces formed at LT and compare this data to that taken from the RT formed interfaces.[11]

a. Ag/HgCdTe

Figure 1 shows the attenuation of the substrate core levels for both the LT and RT interfaces versus Ag overlayer coverage, where the RT data is from our previous work.[11] The Hg 4f, Cd 3d, and Te 3d deep core levels were taken with Mg Kα (hν = 1253.6 eV) and therefore arise more from the bulk (from 15-20 Å depth), whereas the Hg 5d shallow core level was taken using He II (hν = 40.8 eV) and hence comes from the surface (2-3 atomic layers). The similar attenuation rates of the LT deep core levels as a function of Ag overlayer coverage indicate that there no detectable intermixing or Hg loss at the LT Ag/HgCdTe interface. These LT deep core levels also are seen to attenuate at a much faster rate than the RT deep core levels, indicating that the interface formed at LT is much more abrupt than the corresponding interface formed at RT. In addition, escape depth analysis of the LT core levels indicates that these semiconductor core levels attenuate very closely to the rate expected for laminar overlayer coverage. However, the LEED pattern taken at the LT surface does not completely disappear until ~ 8ML, which suggests that some degree of Ag clustering may be occurring at low coverages, but the rapid attenuation rate at low coverages of the surface sensitive Hg 5d core level closely matches that expected at an abrupt interface. Hence, although clustering may be occurring at the LT Ag interface, this effect must be slight. The different attenuation rates of the RT deep core levels indicate that the RT interface is

highly non-abrupt and intermixed, with the Ag diffusing 100's of Å into the bulk, replacing Hg.[11] Therefore, by lowering the temperature of the HgCdTe substrate during Ag overlayer formation, profound differences in the surface morphology compared to that for the RT case are observed, where a highly abrupt interface with no detectable intermixing is found.

b. Al/HgCdTe

For the case of LT Al/HgCdTe, some Hg loss (< 20% in the top 10-20 Å of the HgCdTe) is evident at 1ML Al coverage, but much less than the 60% observed in the surface region for the RT case at the same coverage. Figure 2 shows the ratio R(Θ) of the Hg4f core level intensity to the Te 3d core level intensity as a function of overlayer Al coverage for the LT and RT [11] interfaces, where $R(\Theta) \equiv I_{Hg4f}/I_{Te3d}$ at overlayer thickness Θ in ML, and R(0) is the ratio of the initial intensities. At an abrupt interface with no Hg loss, this value should remain close to unity[16], but as can be seen for both the LT and RT cases, the Hg signal decreases faster than the Te signal. However, this effect is much more rapid in the RT interface. In both cases, the Te comes out of the lattice and reacts with the Al, but this process is impeded at the LT interface. The LEED pattern disappears by 3 ML for the Al LT growth, which is interpreted as non-crystalline Al covering the slightly disrupted HgCdTe lattice. No LEED patterns were taken on the RT Al/HgCdTe system, but for comparable losses of Hg (60%) at other RT metal/HgCdTe interfaces, the LEED pattern is seen to disappear by 0.5 ML. Hence, the degree of disruption for the LT Al interface is much less than that for the RT case, but most likely much lower temperatures are needed to prevent disruption at the Al/HgCdTe interface.

B. Band Bending

Both of the LT interfaces exhibit unusual band bending at low coverages (< 5ML), but at thicker overlayer coverages the bands remain fixed in energy and approach the values seen at the RT interfaces. Figure 3 shows the He I ($h\nu$ = 21.2 eV) spectra of the Cd 4d and Hg 5d shallow core levels for both LT interfaces at selected overlayer coverages Θ in ML. All of the solid spectra

where taken immediately following the metal depositions. The gray spectra were taken after time in Fig 3a, and after exposure to x-rays in Fig 3b. The details of these gray spectra will be discussed in the next two sections. For both of the cleave surfaces, the binding energy (BE) referred to E_f of the Hg $5d_{5/2}$ is: -8.20 ± 0.05 eV. Taking the valence band maximum (VBM) to be located 7.85 eV above the Hg $5d_{5/2}$ for $Hg_{0.61}Cd_{0.39}Te$ [17], this places E_f approximately 0.35 eV above the VBM, *i.e.* near the conduction band minimum (CBM), since the bandgap $E_g = 0.4$ eV at 170 K for x = 0.39 HgCdTe.[18]

In the following sections we refer to the movement of the bands and of the E_f interchangeably. Since the VBM is tied to the same energy reference scale as the core levels, a uniform movement of the energy centroids of the core levels (*i.e.* all of the core levels moving together) indicates an identical movement in energy of the VBM. Therefore, a movement of the bands to lower BE indicates an upward movement of the VBM with respect to the E_f, or, identically, a downward movement of the E_f towards the VBM. The following two sections discuss the LT Ag and Al cases separately.

a. Ag/HgCdTe

For the spectra taken from the LT Ag/HgCdTe interface shown in Fig. 3a, at the initial coverage shown (Θ = 0.2 ML) the cores shift to deeper BE with respect to the position of the cleave. This indicates that the E_f initially moves higher into the conduction band (CB), *i.e.* E_f - VBM is 0.55 ± 0.05 eV. For all of the evaporation sequences that occur before the cumulative Ag coverage is greater than 5 ML, spectra taken 60 min. after the first spectra show that the core level energies have shifted back to the values seen at the cleave. One of these cases is shown in Fig. 3a, where, for Θ = 0.5 ML, retaking the spectra for the 0.5 ML coverage (gray curve) 60 min. after the initial spectra (solid curve) reveals that the core levels have shifted back to the initial cleaved position, thus indicating that E_f has moved back to the level seen initially at the clean-cleaved surface. As the Ag coverage increases, spectra taken immediately after the Ag deposition show

that E_f moves less and less into the CB until, for thicker Ag coverages, E_f goes to slightly below (~0.05 eV) the cleave position, or 0.30 ± 0.05 eV above the VBM. This final position is still above the intrinsic Fermi level for 0.40 eV bandgap, therefore the surface is still *n*-type, but the Ag has a slight *p*-type doping effect in the semiconductor. It is interesting to note that for the x = 0.23 HgCdTe sample studied in the RT case[11], the final position of E_f was also 0.05 eV below the initial cleaved position. Although no intermixing is detectable from the spectra giving rise to Fig. 1, these band bending results suggest highly that some Ag diffuses into the bulk. To cause a movement of E_f towards *p*-type, concentrations of Ag on the order of 10^{18}-10^{19} cm^{-3} are needed in the surface region of the HgCdTe, which is well below the detectability of XPS.

b. Al/HgCdTe

For the LT Al case shown in Fig. 3b, the core levels do not exhibit a shift with time as in the LT Ag case, but a shift is observed after exposure of the surface to a Zr x-ray source. For the initial coverage of 0.1 ML (shown in Fig. 3b, solid curve), the core levels move 0.25 eV to deeper BE, or E_f goes to 0.60±0.05 eV above the VBM. After exposure to a Zr x-ray source, a slight shift of the core levels to lower BE (gray curve) occurs, indicating that E_f moves back toward the level seen at the cleaved surface. As the Al coverage increases, the core level shifts after x-ray source exposure become less. At higher Al coverages, the core levels remain at the initial position reached at 0.1 ML, even after exposure to the x-ray source. Hence for thicker coverages, E_f stays at ~0.60 eV above the VBM for the LT Al/HgCdTe interface (in agreement with the RT cases).[11-13] Thus, Al is seen to dope the surface *n*-type, but the position change of E_f after x-ray exposure for low coverages suggests that some defect level is being created at the surface during the x-ray exposure.

C. Interface Stability

The question arises as to whether these interfaces are stable to overlayer/substrate intermixing when warmed up to room temperature. For the LT Ag case, "annealing" the interface

at RT for 30 min. reveals that the interface is unstable, but for the LT Al case, nothing happens when the interface is annealed to RT, indicating that the LT Al/HgCdTe interface exhibits stability when warmed to RT. Figure 4 shows He I spectra of the Hg 5d, Cd 4d, Ag 4d shallow core levels at 12 ML Ag coverage before and after a 30 min. RT anneal. The spectra have been offset to facilitate comparison. The major spectral feature changes after annealing are: an increase in the Cd 4d and Hg 5d core levels intensities and a shift to lower binding energy by 0.1 eV, a decrease in the Ag 4d intensity and its width but no shift in the energy centroid, and a smoothing of the step at E_f. An increase of the Hg and Cd core level intensities could be due either Ag diffusing into the bulk causing the thickness of the Ag overlayer to decrease, or the Ag clustering at the surface which would expose some of the substrate. Because the Ag 4d intensity decreases as a result of the anneal, the Ag diffusing into the bulk seems to be more consistent with these observations. In addition, the shift of the Hg and Cd core levels ~0.1 eV to lower binding energy dictates that E_f moves 0.1 eV toward the VBM, which is consistent with the *p*-type dopant Ag doping the semiconductor. The narrowing of the Ag 4d core levels also indicates that the Ag overlayer changes its properties as a result of the annealing process. Therefore the spectra in Fig. 4 show very graphically the instability of the LT formed Ag/HgCdTe interface to intermixing upon annealing at RT.

IV. CONCLUSIONS

Lowering the temperature of the HgCdTe substrate during metal overlayer growth reduces the degree of intermixing between the substrate and the metal overlayer. At the non-reactive LT Ag/HgCdTe interface, no detectable intermixing is observed as Ag is deposited to form the interface, but when warmed to RT, the interface is unstable to Ag/HgCdTe intermixing. At the more reactive Al/HgCdTe interface, the degree of intermixing and Hg loss is greatly reduced at LT, but Hg loss is still seen. For both systems at low metal coverages, unusual band bending behavior is observed. The bands move with time after deposition is completed for the Ag case but only after

x-ray exposure for the Al case. For Ag case at high coverages, the position of the surface Fermi level remains fixed at 0.05 eV below its initial position at the cleave, and for the Al case, the final position of the surface Fermi level is 0.30 eV above the initial cleaved position. The final positions of E_f of both these LT cases are in agreement with their corresponding RT cases.

ACKNOWLEDGEMENTS

*This work is supported by DARPA contract # N00014-86-K-0854.

REFERENCES

a) Stanford Ascherman Professor of Engineering.

1 G. D. Davis, Vouto **16**, 127 (1986), and references therein.

2 D. J. Friedman, G. P. Carey, I. Lindau, and W. E. Spicer, J. Vac. Sci. Technol. A **5** 3190 (1987) , and references therein.

3 D. J. Friedman, G. P. Carey, I. Lindau, and W. E. Spicer, Phys. Rev. B., **34** 5329 (1986) .

4 G. P. Carey, D. J. Friedman, I. Lindau, and W. E. Spicer, J. Vac. Sci. Technol. A **5** 3198 (1987).

5 A. Sher, A.-B. Chen, W. E. Spicer, and C. K. Shih, J. Vac. Sci. Technol. A **3**, 105 (1985).

6 W. E. Spicer, D. J. Friedman, G. P. Carey, J. Vac. Sci. Technol. A, in press.

7 A. Wall, A. Raisanen, S. Chang, P. Philip, N. Troullier, A. Franciosi, and D. J. Peterman, J. Vac. Sci. Technol. A **5** 3192 (1987).

8 A. Raisanen, A. Wall, S. Chang, P. Philip, N. Troullier, A. Franciosi, J. Vac. Sci. Technol. A, in press.

9 G. D. Davis, W. A. Beck, M. K. Kelly, D. Kilday, Y. W. Mo, N. Tache, and G. Margaritondo, J. Vac. Sci. Technol. A, in press.

10 K. C. Mills, *Thermodynamic Data for Inorganic Sulphides, Selenides, and Tellurides* (Butterworths, London, 1974).

11 D. J. Friedman, G. P. Carey, C. K. Shih, I. Lindau, W. E. Spicer, and J. A. Wilson, J. Vac. Sci. Technol. A **4**, 1977(1986).

12 D. J. Friedman, G. P. Carey, C. K. Shih, I. Lindau, W. E. Spicer, and J. A. Wilson, Appl. Phys. Lett. **48**, 44 (1986).

13 G. D. Davis, W. A. Byer, R. A. Riedel, and G. Margaritondo, J. App. Phys. **57**, 1915 (1985).

14 I. S. Birt, V. I. Kempnik, and D. I. Tsyutsyura, Inorg. Mater. **22**, 1228 (1986).

15 J. A. Silberman, P. Morgen, I. Lindau, W. E. Spicer, and J. A. Wilson, J. Vac. Sci. Technol. **21**, 154 (1982).

16 Actually this value would increase slightly over unity due to the escape depth differences in the Hg 4f and Te 3d electrons (escape kinetic energies of 1144 and 666 eV, respectively), with the escape depth of electrons coming from Te 3d being less than that of Hg 4f electrons.

17 Determined from measurements performed on HgCdTe with angle-resolved photoemission spectroscopy.

18 G. L. Hansen, J. L. Schmit, T. N. Casselman, J. Appl. Phys. **53**, 7099 (1982).

Figure Captions

Figure 1 The HgCdTe core level intensity as a function of Ag overlayer thickness. The attenuation of the LT core levels as a function of Ag overlayer coverage is much faster and uniform than the corresponding RT case. The LT core levels attenuate at a rate expected for an abrupt interface with a laminar coverage of Ag on the HgCdTe, indicating that there is no detectable intermixing or Hg loss at the LT Ag/HgCdTe interface. The Hg 5d core level attenuates at a more rapid rate due to the minimized escape depth of these electrons.

Figure 2 The figure on the right shows the ratio $R(\Theta)$ of the Hg4f core level intensity to the Te 3d core level intensity as a function of overlayer Al coverage for the LT and RT interfaces, where $R(\Theta) \equiv I_{Hg4f}/I_{Te3d}$ at overlayer thickness Θ in ML, and R(0) is the ratio of the initial intensities. The Hg signal decreases faster than the Te signal in both cases, but the effect is much more rapid in the RT interface.

Figure 3 He I spectra showing the Hg 5d and Cd 4d shallow core levels as a function of overlayer coverage Θ in ML. For the LT Ag case shown in (a), retaking the spectra for the 0.5 ML coverage (gray curve) one hour after the initial spectra (solid curve) reveals that the core levels have shifted back to the initial cleaved position. At thicker coverages, E_f stays 0.30 eV above the VBM. For the LT Al case shown in (b), the BE does not exhibit a shift with time as in the LT Ag case, but a shift is observed after exposure of the surface to a Zr x-ray source. An example of this is seen at 0.1 ML coverage, where a slight shift of the core levels to lower BE (gray curve) occurs after exposure to the X-ray source, indicating E_f moves back toward the level seen at the cleaved surface. For thicker coverages, E_f stays at 0.60 eV above the VBM.

Figure 4 He I spectra of the Ag/HgCdTe interface at 12 ML coverage showing the effect of annealing the interface at RT for 30 min. The Hg 5d, Cd 4d, and Ag 4d shallow core levels change in intensity and the semiconductor constituents shift in energy. The step defining the position of the Fermi level also becomes less defined.

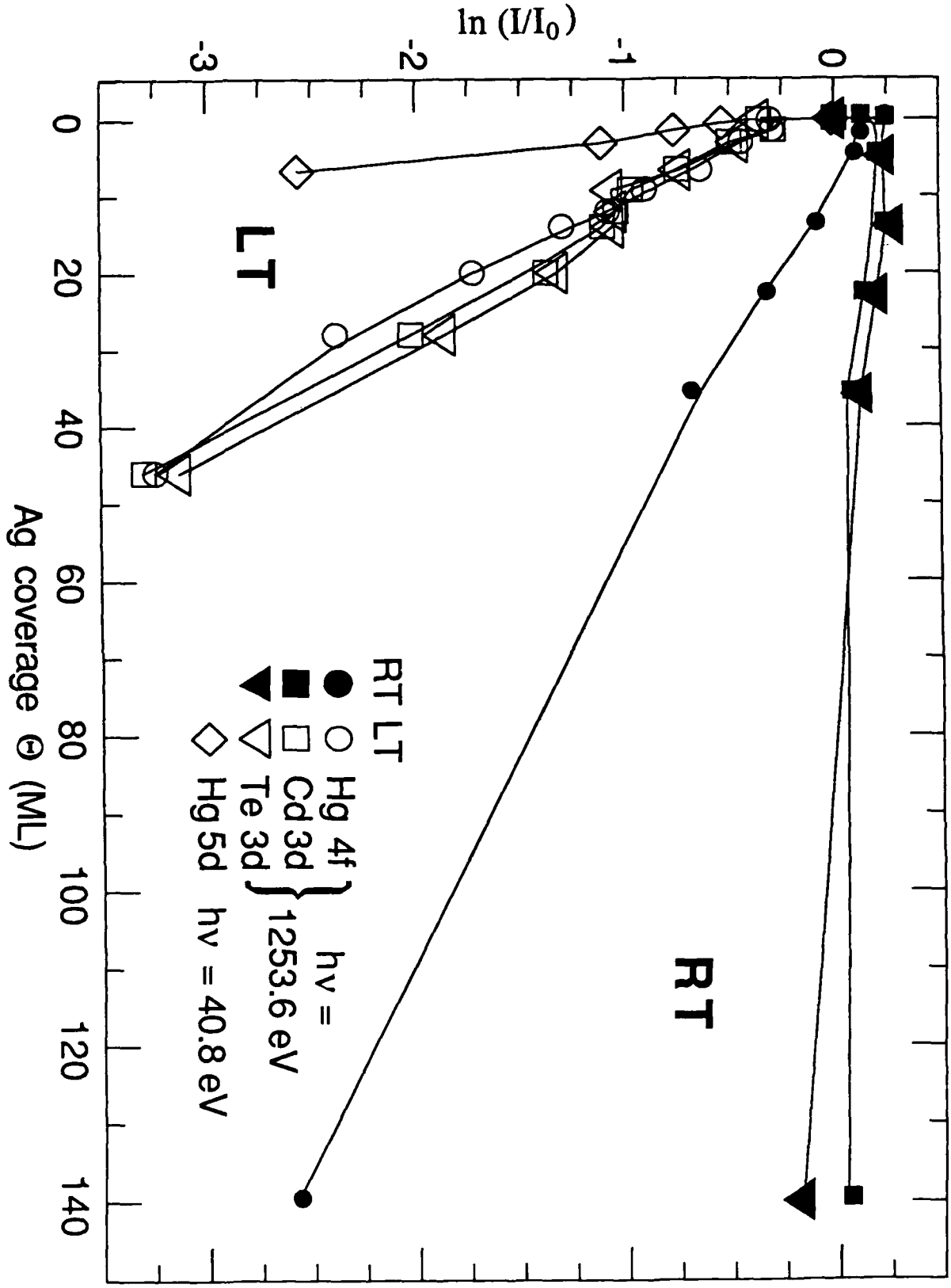
ln (I/I0)
-3
-2
-1
0
0
20
40
60
80
100
120
140
Ag coverage Θ (ML)
LT
RT
RT LT
Hg 4f
Cd 3d
Te 3d
hv = 1253.6 eV
Hg 5d hv = 40.8 eV

Figure 1

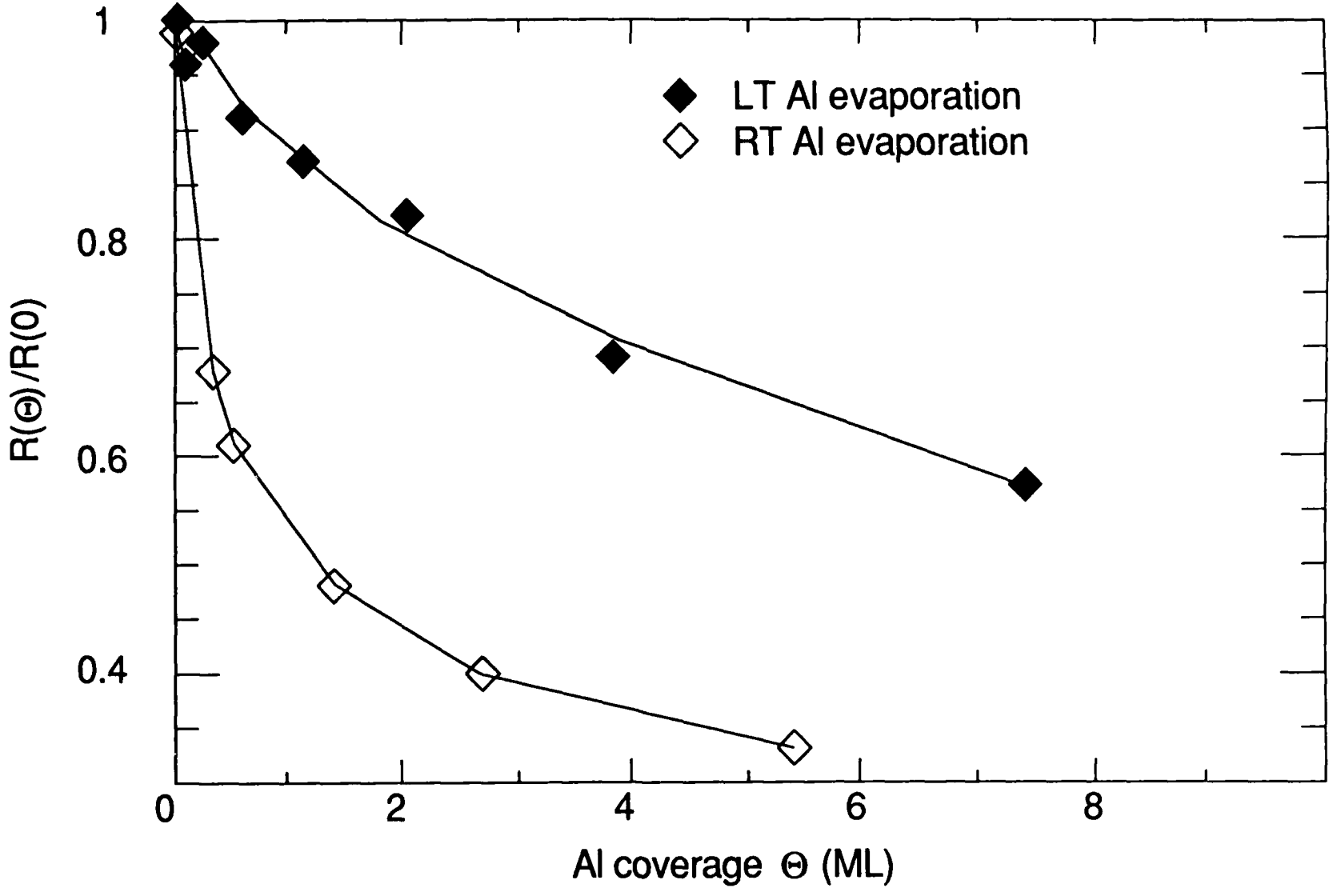
1
0.8
0.6
0.4
R(Θ)/R(0)
LT Al evaporation
RT Al evaporation
0
2
4
6
8
Al coverage Θ (ML)

Figure 2

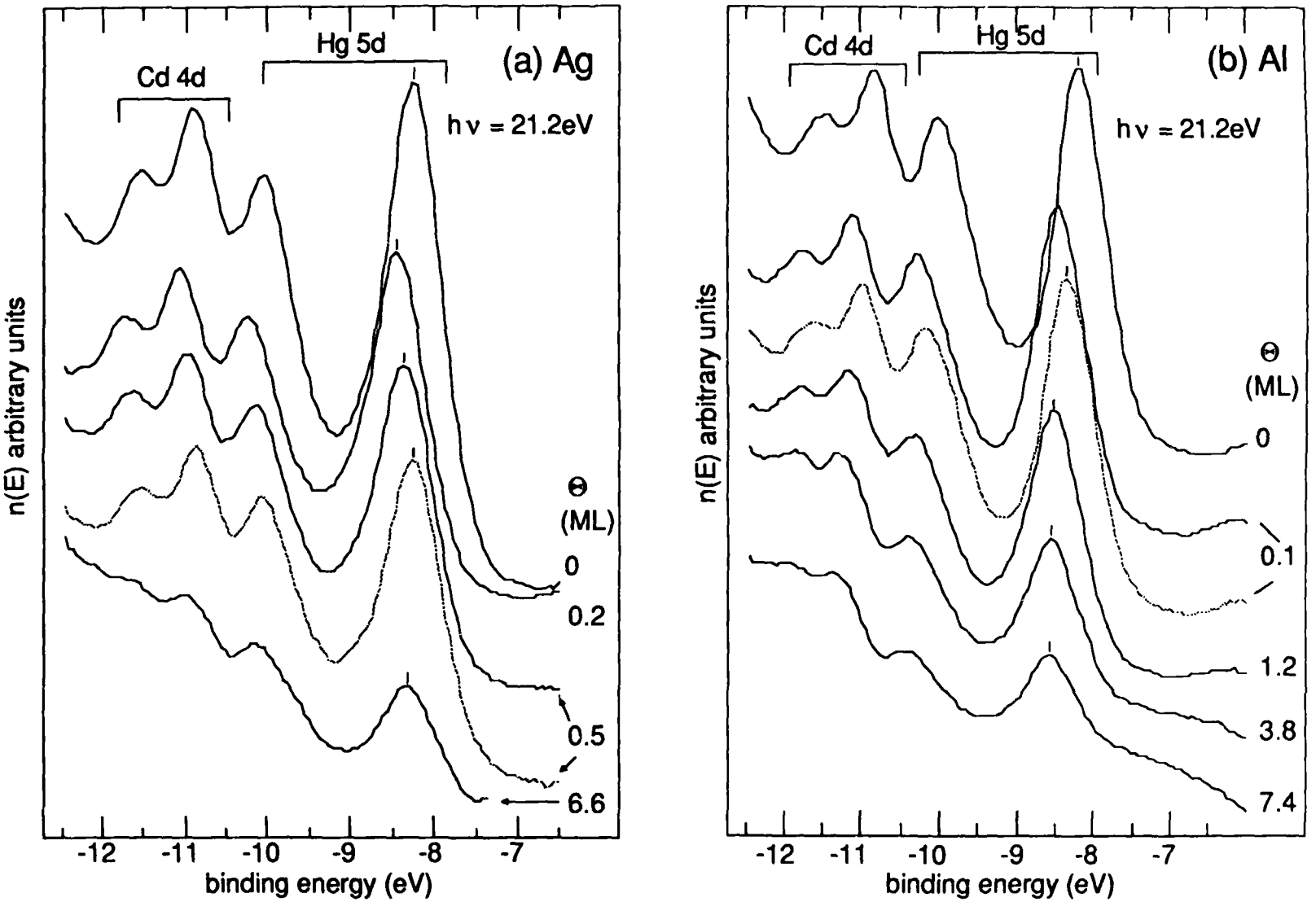
Cd 4d
Hg 5d
(a) Ag
hν = 21.2eV
n(E) arbitrary units
Θ
(ML)
0
0.2
0.5
6.6
-12
-11
-10
-9
-8
-7
binding energy (eV)
Cd 4d
Hg 5d
(b) Al
hν = 21.2eV
n(E) arbitrary units
Θ
(ML)
0
0.1
1.2
3.8
7.4
-12
-11
-10
-9
-8
-7
binding energy (eV)

Figure 3

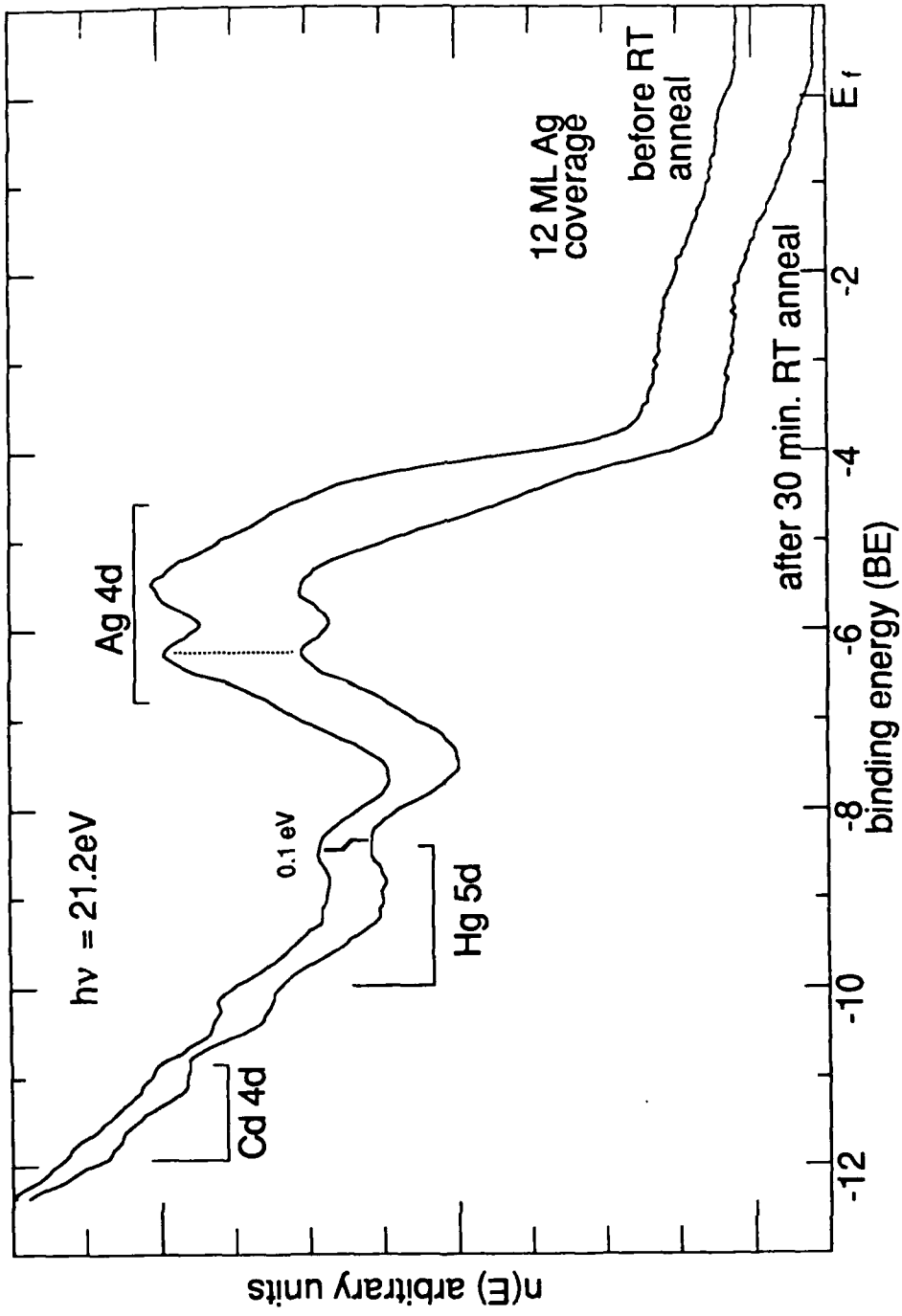
n(E) arbitrary units
hν = 21.2eV
Cd 4d
Ag 4d
0.1 eV
Hg 5d
12 ML Ag coverage
before RT anneal
after 30 min. RT anneal
E_f
-12
-10
-8
-6
-4
-2
binding energy (BE)

Figure 4

Section IV - Noble Metals on CdTe

I. INTRODUCTION

In the study of metal/semiconductor interfaces, the morphology of the interface is of interest both intrinsically, since the driving forces behind the observed interfacial chemistry are still not fully understood, and also because of the interplay between interface morphology and Schottky barrier height. Studying the interfaces with II-VI semiconductors such as CdTe is also of relevance to III-V semiconductor interface research, as the greater ionicity of the II-VI semiconductor provides insight into the role of cation-anion bonding in interface formation [1]. This paper presents a photoemission study of noble metal interfaces with CdTe: more specifically, the Au/p-CdTe, Ag/n-CdTe, Cu/n-CdTe, and Cu/p-CdTe interfaces. Bulk thermodynamic data relevant to the determination of the interface morphology are given in Table I, which shows heats of metal-telluride formation from Ref. [2] as well as calculated heats of alloying ΔH_{sol}(Cd;M) of Cd at infinite dilution in the overlayer metals (M).

CdTe is not only of practical interest, for instance for solar cell technology, but also serves as a prototypical II-VI semiconductor for the purposes of interface research. Previous studies[3]-[5] of metal interfaces with the cleaved CdTe(110) surface have tended to concentrate more on the Schottky barrier height than on the interface morphology, while both will be emphasized in this paper. Finally, studying the metal/CdTe interface is helpful in understanding the more complex metal/$Hg_{1-x}Cd_xTe$ interface, in which there has recently been increasing interest.[6]-[12] $Hg_{1-x}Cd_xTe$ (MCT), a pseudobinary alloy with a bandgap[13] varying from 0 to 1.50 eV (at 300 K) as the composition is varied from x=0 to 1, is of technological importance as an infrared detector. Related to the variable band gap is a marked instability in the Hg-Te bond,[14] which in turn plays a crucial role in metal/MCT interface properties. A comparison with the corresponding metal/CdTe interfaces will thus assist in the understanding of the role of the Hg bond in metal/MCT interface formation.

II. EXPERIMENTAL

Single-crystal bars of CdTe (p-type for the Au/CdTe study and n-type for the Ag/CdTe and Cu/CdTe studies) with cross-sectional areas of ~5×5 mm^2 were transferred into a previously-baked vacuum chamber and then cleaved in ultra-high vacuum (base pressure less than 1×10^{-10} torr) to reveal a (110) face. Sequential depositions of metal were performed onto the room temperature surface from a tungsten filament, with overlayer thicknesses monitored with a quartz crystal microbalance. The amount of metal deposited is given in units of Å and monolayers (ML), which we define to be the surface density of atoms on the CdTe (110) face: 1 ML=6.76×10^{14} atoms/cm^2 which corresponds to 1.15 Å of metallic Au, 1.15 Å of metallic Ag, and 0.80 Å of metallic Cu. The ML is the more appropriate unit for low coverages. The surface was studied at each coverage by X-ray and ultraviolet photoelectron spectroscopy (XPS and UPS) using respectively a Mg Kα X-ray source (hν=1253.6 eV) and a helium lamp (He I and He II, hν=21.2 and 40.8 eV); the photoelectrons were analyzed with a double-pass cylindrical-mirror analyzer (CMA).

III. RESULTS: Au/p-CdTe

A. Overlayer adsorption

Figures 1(a) and 2 show He I spectra of the valence band and the Cd 4d shallow core level as a function of Au deposition. From the spectral region near the Fermi level E_F, shown in the inset of Fig. 1, it can be seen that by Θ=0.5 ML there is clear emission to E_F; a metallic Fermi edge can be detected by Θ=2-4 ML. The occurrence (implied by the presence of the Fermi edge) of some fraction of the overlayer in the metallic state at a coverage as low as 2 ML suggests that at this coverage the deposited Au has formed clusters (possibly containing Cd or Te atoms dissociated from the semiconductor surface) large enough to support a Fermi surface.

By 1 ML coverage, emission from the Au 5d states is visible in the spectra; as more metal is deposited, the Au 5d spectrum undergoes a ~0.2 eV shift to higher kinetic energy. A similar shift (~0.4 eV to higher kinetic energy, mostly completed by Θ= 10 ML) also occurs in the Au 4f states. The higher Au 4f binding energy at the lowest coverages is consistent with either Au

adsorption as a reacted Au-Te phase or with the cluster formation mentioned above, as clusters would have a higher binding energy than the pure metal.[15]

The valence band spectrum undergoes a continuous evolution in shape, approaching a stable lineshape by about Θ=10 ML. This lineshape, while dominated by emission from Au-derived states, does not quite correspond to the lineshape of elemental Au, as can be seen from Fig. 1(b) which compares the valence band spectrum of 20 Å (17 ML) Au/CdTe with an Au/stainless steel reference spectrum. Since the He I spectrum probes only the top 10-20 Å of the surface, we take the departure of the 20 Å Au/CdTe valence band from that of pure Au to indicate the presence of Cd and/or Te dissociated from the semiconductor and intermixed into the overlayer.

B. Te dissociation

The presence of significant quantities of a semiconductor component in the overlayer would result in a greater photoemission intensity from that component than would be observed for an abrupt laminar overlayer. Figure 3(a) plots the attenuation with overlayer coverage of the Cd and Te core level intensities I, normalized to their zero-coverage values I_0. Below about 30 Å coverage, the Te 3d signal attenuates roughly in exponential form with a rate corresponding to an escape length of about 20-25 Å, consistent with a reasonably abrupt interface. However, above about 30 Å coverage the Te intensity starts to level off, so that even at 200 Å it is still about 15% of its initial intensity. This lack of attenuation is too pronounced to be attributable entirely to islanding (although some degree of islanding cannot be explicitly ruled out), and thus provides an unambiguous signature of the presence of Te in the overlayer.

The Te 3d and 4d core levels excited by Mg Kα light appear respectively at 670 eV and 1200 eV kinetic energy, so that the Te 4d probe is more bulk-sensitive. Defining the escape lengths for Te 3d and Te 4d photoelectrons as λ_{3d} and λ_{4d} respectively, then $\lambda_{4d} > \lambda_{3d}$ due to the higher kinetic energy of the Te 4d photoelectrons.[16] Thus, comparison of the attenuation with overlayer deposition of the Te 3d and 4d core intensities can provide information on the distribution of Te in the overlayer. Figure 3(b) shows the intensity ratio $R(\Theta) \equiv I_{Te3d}(\Theta)/I_{Te4d}(\Theta)$

normalized to the zero-coverage value R(0). If the dissociated Te were distributed uniformly throughout the overlayer (at a density less than in bulk CdTe), R(Θ) would decrease with increasing overlayer coverage. However, Fig. 3(b) shows that at Θ≈30 Å, R(Θ)/R(0) starts to rise, reaching a value of about 1.3 by 100 Å coverage. This increase in the more surface-sensitive Te 3d signal relative to the Te 4d indicates that most of the dissociated Te is within roughly the Te 3d escape length λ_{3d} of the surface, so that the Te 3d signal is more dominated by the dissociated Te than is the less surface-sensitive Te 4d signal. Thus, the difference in Te 3d and Te 4d attenuation rates indicates the development of a Te-rich layer segregated at or near the surface of the overlayer, as opposed to a uniform distribution of Te in the overlayer. A comparison of Figs. 3(a) and 3(b) shows that R(Θ)/R(0) starts to rise at the same coverage (~30 Å) at which the Te attenuation rate starts to slow from its original "abrupt-like" rate. Thus, the onset of large-scale Te dissociation occurs at about 30 Å coverage, and as the Te is pulled from the surface of the semiconductor above this coverage it is segregated towards the surface of the overlayer.

It was shown in Sec. III-A above that the Au within a photoelectron escape length (20-30 Å) of the surface of the overlayer is not in pure elemental form even at high coverages. The much faster attenuation and consequent lower signal intensity at high coverages of the Cd 3d compared to the Te 3d, as seen in Fig. 3(a), implies that the Cd concentration in the near-surface region of the overlayer is negligible compared to the Te concentration. The evolution of the Te 3d and Au 4f core level widths with coverage, reflecting the chemical interaction of these two elements as the interface is formed, is shown in Fig. 4. As metal is deposited upon the semiconductor, the Te signal, which at zero coverage arises solely from Te in the CdTe lattice, acquires contributions from Te bound to Au, probably with several kinds of inequivalent lattice sites, and the width of the total XPS Te 3d signal increases. Conversely, the width of the Au signal drops with increasing coverage, as the distribution of the number of Te atoms seen by a given Au atom becomes more uniform with increasing coverage. Furthermore, cluster size effects, which play an important role in the overlayer metal's core level binding energy at low coverages and small cluster sizes, become less important with increasing coverage and larger cluster sizes.

C. Cd dissociation and band bending

As reflected in the Cd 4d core levels in Fig. 2, between zero coverage and Θ=0.1 ML there is a rigid shift of the energy bands 0.15±0.05 eV to higher binding energy. Using the value of $E(Cd\ 4d_{5/2}) - E_{VBM} = -10.3$ eV in CdTe,[17] the result of this initial band bending is to put the Fermi level 0.8±0.1 eV above the valence band maximum at Θ=0.1 ML. However, the band bending behavior at higher coverages is not immediately clear: the band bending may be deduced only from the substrate photoelectron signal, which must therefore be deconvolved from contributions which may arise from dissociated Cd or Te atoms intermixed into the overlayer. Thus, while Fig. 2 appears to show a gradual shift of the Cd 4d core level to higher kinetic energy which might at first glance be interpreted as being due to further band bending, the possibility must be considered that what is instead being observed is an increasingly intense contribution, at higher kinetic energy than the substrate peak, from dissociated Cd. Thus the question of Cd dissociation is important not only for understanding the morphology of the interface, but also for determining the band bending and consequently the Schottky barrier height due to the interface.

The attenuation of the Cd 4d intensity at $h\nu$=40.8 eV, shown in Fig. 3(a), is much too slow to be consistent with an abrupt laminar interface, since at $h\nu$=40.8 eV the Cd 4d core level appears at a kinetic energy of about 25 eV with a corresponding photoelectron escape length on the order of 5 Å. Taken by itself, the Cd 4d attenuation rate is thus consistent with Cd dissociation or with cluster formation of the overlayer, which would also result in a reduced attenuation rate of the Cd signal intensity. Less ambiguous evidence for the influence of dissociated Cd in the Cd 4d signal is provided by a comparison of the Cd 4d (He II light) and Cd 3d (Mg Kα light, kinetic energy ~840 eV) centroids, shown in Fig. 5. The variation of photoelectron escape length with kinetic energy is discussed in Ref. [16]. Because the Cd 3d signal is much more bulk sensitive (photoelectron escape length ~20 Å) than the Cd 4d signal (escape length ~5 Å), at coverages below about 10 Å the Cd 3d signal will be dominated by the substrate contribution, and thus will be a much better indicator of the substrate's band bending than the Cd 4d signal would be. The

levelling off of the Cd 3d peak position from low coverages all the way up to the highest coverage (10-20 Å) for which the Cd 3d signal is still dominated by the substrate, indicates that the band bending is indeed complete at monolayer coverages, and that the drift of the Cd 4d signal to lower binding energy is in fact due to increasing contribution from dissociated Cd. It should be noted that Patterson and Williams[5] reported no Cd dissociation in their studies of the Au/n-CdTe interface, although their photoelectron spectra are in fact consistent with ours.

The binding energy of the dissociated cation core level can give information concerning the chemical environment seen by the dissociated species.[18] In the present case there are essentially three possibilities: the dissociated Cd may be segregated in pure metallic form, it may be alloyed with the Au overlayer, or there may be some dissociated Te in its local environment as well. Pure metallic Cd has a $4d_{5/2}$ binding energy of -10.6 eV,[19] while the binding energy for Cd alloyed in Au will be shifted from this pure metal value by an amount which can be calculated[18],[20] from a Born-Haber cycle argument using as inputs the heats of solution given by the Miedema semi-empirical model.[21] For Cd at infinite dilution in Au, this method predicts[12] an alloy shift of 0.11 eV to lower binding energy from the pure Cd metal binding energy. The observed Cd 4d core level position above 60 Å, at which coverages the Cd signal should be completely dominated by the dissociated component, gives a binding energy of -10.75±0.05 eV below E_F for the dissociated Cd $4d_{5/2}$. This binding energy is thus about 0.1 eV higher than the pure metallic binding energy, and 0.2 eV higher than the predicted energy for Cd alloyed in Au. The smallness of these differences, combined with the uncertainty in the alloy shift calculation, does not permit either possibility to be completely ruled out. However, it should be noted that the third possibility noted above, i.e. the presence of the more electronegative Te in the local environment of the dissociated Cd, would be expected to shift the Cd binding energy toward higher binding energy, fully consistent with what is observed. A similar behavior has been seen for dissociated Cd in the $Cu/Hg_{1-x}Cd_xTe$ interface.[9]

D. Schottky barrier formation

Having shown that in fact the band bending is finished by $\Theta \approx 1$ ML, we deduce a final Fermi level position of $E_F - E_{VBM} = 0.8 \pm 0.1$ eV, implying a Schottky barrier height of ~0.8 eV to the p-type sample. A comparison with other experimental results is given in Sec. VI-B.

IV. RESULTS: Ag/n-CdTe

A. Overlayer adsorption

He I spectra of the valence band region with increasing coverage of Ag on the semiconductor substrate are shown in Fig. 6. In the region near E_F, shown on an expanded scale in the inset of the figure, there is emission extending to E_F by the initial coverage of 0.1 ML, while a metallic Fermi edge is detectable by Θ=1-2 ML. As in the case of Au overlayers discussed above, the presence of a Fermi edge at such low overlayer coverages strongly suggests that the overlayer metal is forming clusters on the surface rather than covering the surface laminarly.

With increasing coverage, Ag 4d states centered at about 5.5 eV below E_F arise in the valence band spectrum; the shape of the Ag 4d line has essentially stabilized by 4 ML coverage, with further depositions resulting in an increased Ag 4d intensity but little further change in spectral shape. A similar evolution takes place for the Ag 3d core level: between Θ=0.1 and 4 ML the Ag 3d peak position shifts 0.2-0.3 eV to higher kinetic energy, stabilizing above the 4 ML coverage at a binding energy of -368.3±0.1 eV for the Ag $3d_{5/2}$ component. As with Au/CdTe, the shift of the overlayer metal core level to lower binding energy with increasing (low) coverage may represent cluster size effects due to increasing cluster size at higher coverages, or changes in the degree of chemical interaction with the semiconductor substrate.

B. Semiconductor dissociation

The evolution of the Cd 4d core levels with Ag deposition is shown in the He I spectra of Fig. 7. In contrast to the cases of Au/CdTe and Cu/CdTe (see Sec. V), for Ag/CdTe there is clearly no dissociated Cd component visible in the spectra, consistent with the observations of

Patterson and Williams.[5] Thus the Cd spectra in Fig. 7 originate from the semiconductor substrate, and can therefore be used to extract the band bending behavior as discussed below in Sec. IV-C. Furthermore, the identification of the Cd 4d spectra as originating from the substrate, combined with the relatively slow attenuation of these spectral intensities with increasing overlayer coverage, provides information on the growth morphology of the overlayer. The slowness of the Cd attenuation rate is shown more clearly in Fig. 8, which shows the semiconductor core level intensities I normalized to their zero-coverage values I_0. The Cd 4d's at hν=40.8 eV attenuate by 35 Å coverage to I/I_0≈5%, corresponding to an equivalent exponential escape length of about 12 Å, roughly double what one would expect for He II spectra of the Cd 4d's (kinetic energy ~25 eV). Because this slow attenuation cannot be attributed to Cd dissociation and intermixing with the overlayer, it implies that the overlayer distribution on the semiconductor surface is clustered rather than laminar even at coverages as high as 35 Å. Significant clustering of Ag on a CdTe(100) surface prepared by sputter-anneal cycles has been observed by John *et al.*[22]

The attenuation of the Te intensity (also shown in Fig. 8) slows greatly above Θ=35 Å and almost levels off by Θ=200 Å. If this lack of attenuation were due solely to clustering of the overlayer, the Cd and Te intensities would attenuate at roughly the same rate.[23] However, as shown in Fig. 8, such behavior is not observed; instead, by Θ=200 Å the relative attenuation for the Cd 3d core intensity is about ten times greater than for the Te 3d. Therefore, the attenuation of the Te intensity cannot be attributed entirely to clustering of the overlayer and must be due in large part to Te dissociating from the semiconductor and intermixing with the overlayer. The dissociation of Te from the CdTe surface implies the production of dissociated Cd as well. Since no dissociated Cd is observed directly in the photoemission spectra, the dissociated Cd must be localized near the interface under the Ag overlayer, providing a negligible contribution to the spectra, in contrast to the dissociated Te which diffuses out to the overlayer near-surface.

By 100 Å coverage the Te $4d_{5/2}$ binding energy has decreased to -39.9 eV relative to the Fermi level. In elemental Te, $E(\text{Te } 4d_{5/2}) - E_{VBM}$ = -40.5 eV,[24] which, assuming E_F does not acquire a degenerate position below the Te VBM, implies $E(\text{Te } 4d_{5/2}) - E_F \geq$ -40.5 eV for

elemental Te. Since the observed Te binding energy is 0.6 eV lower than this, the dissociated Te at the Ag/CdTe interface must be in reacted form. Elementary (if perhaps naive) charge transfer considerations would predict a shift from the elemental Te binding energy to lower binding energy for Te bound to a cation such as Ag; the observed shift is indeed in this direction.

Examination of the binding energy region within 4 eV of E_F shows a feature, peaked at -2.5 eV for coverages below 6 ML, which shifts 0.5 eV to higher kinetic energy and decreases in intensity and sharpness with increasing Ag coverage. This feature, which is still visible beyond 60 Å coverage, does not correspond to any spectral feature of Ag metal and instead arises from Te-derived p-like valence states. At high coverages, where the substrate is no longer visible to UPS, this feature originates from dissociated Te in the overlayer.

In contrast to our results, the John *et al.* study[22] shows no evidence for Te dissociation from the semiconductor, but does find Cd floating on the Ag overlayer islands. However, the different surface orientation, CdTe(100), and surface preparation, sputter-anneal cycling, result in an initial semiconductor surface sufficiently different from ours that the different interface morphology is easily understood. Their zero-coverage surface is Cd-terminated, and covered with an additional quarter-ML of excess Cd; the combination of these two factors seems likely to suppress the Te dissociation that we observe for the stoichiometric CdTe(110) surface. These differences serve to emphasize the importance of surface orientation and preparation upon the morphology of subsequently prepared interfaces.

C. Schottky barrier formation

Using the value of $E(Cd\ 4d_{5/2}) - E_{VBM} = -10.3$ eV in CdTe,[17] the cleaved surface Fermi level is located 1.1±0.1 eV above the valence band maximum; i.e. it is pinned 0.4 eV below the conduction band minimum for the n-type sample. Upon Ag deposition, E_F shifts down towards the VBM by 0.1-0.15 eV, as reflected in the corresponding shift to higher kinetic energy of the Cd 4d states in Fig. 7. The final position of E_F is thus 0.95±0.1 eV above the VBM, implying a

Schottky barrier height of about 0.55 eV to the n-type sample. A comparison with other experimental results is given in Sec. VI-B.

V. RESULTS:Cu/CdTe

We summarize here the morphology and band bending of the Cu/n-CdTe interface, which was discussed in detail in Ref. [9]. We also give results for band bending at the Cu/p-CdTe interface.

A. Morphology

Upon Cu deposition, a well-resolved shifted Cd 4d peak originating from dissociated Cd appears in addition to the peak due to metallic Cd; the dissociated Cd peak is the dominant one by 20 Å coverage. Consideration of the attenuation rate of the dissociated Cd signal shows that the dissociated Cd is distributed throughout the overlayer, rather than being segregated at the semiconductor surface. Starting at about 10-15 Å coverage, a significant degree of Te dissociation occurs. The dissociated Te is concentrated largely in a 2-8 Å thick reacted Cu-Te layer within a few Å of the surface of the overlayer; formation of this Te-rich layer is largely complete by Θ=80 Å.

B. Schottky barrier formation

The cleaved surface Fermi level position in the Cu/n-CdTe study was found to lie 1.2±0.1 eV above the VBM, i.e. pinned 0.3 eV below the CBM. Upon Cu deposition, E_F shifted down towards the VBM by ~0.2 eV. This shift, complete by the initial deposition of 0.1 ML, puts the final position of E_F at 1 eV above the VBM, i.e. 0.5 eV below the CBM, giving a Schottky barrier height of ~0.5 eV to the n-type sample. For Cu/p-CdTe, Cu deposition shifted the surface Fermi level up from its cleaved-surface pinning position 0.5±0.1 eV above the VBM to a final position 0.9±0.1 eV above the VBM, giving a Schottky barrier height of ~0.9 eV to the p-type sample. A comparison with other experimental results is given in Sec. VI-B.

VI. DISCUSSION

A. CdTe interface morphology

The most striking behavior common to the three noble metal/CdTe interfaces is the significant motion of dissociated Te from the semiconductor into the overlayer, so that Te is easily detectable in the overlayer near-surface region at coverages well above 100 Å. For Cu and Au overlayers, this dissociated Te is segregated in a Te-rich layer near the surface of the overlayer. A similar analysis could not be performed for the Ag/CdTe interface as the Te 3d/Te 4d core level intensity ratio was not monitored in this case; however, the similarity in the attenuation behavior of the Te 4d for Ag overlayers with the attenuation for Au and Cu overlayers suggests that the dissociated Te in the Ag overlayer may well be concentrated near the surface as it is for the other two noble metal overlayers.

For Ag and Cu, and possibly Au, the dissociated Te from the semiconductor is in reacted form with the overlayer metal. The dissociation of Te from the CdTe substrate and subsequent reaction with the overlayer metal, appears inconsistent with the bulk thermodynamic data of Table I, which shows the CdTe bond strength to be much greater than that any of the noble metal-CdTe compounds. As always, surface and interface effects must be considered along with the bulk thermodynamics. For instance, the heat of condensation of the overlayer metal on the semiconductor could well provide some of the energy needed for dissociation of Te from the CdTe substrate. Once the dissociation has been accomplished, the next step of reaction with the overlayer is favored by bulk thermodynamics.

For Au and Cu overlayers, but not for Ag overlayers, there is dissociated Cd in the overlayer near-surface. Examination of the ΔH_{sol}(Cd;M) values from Table I shows that Cd has a high negative enthalpy of solution in Au, which would tend to favor dissociated Cd being pulled into the overlayer. However, while both Cu and Ag have similar small enthalpies of solution for Cd, only for the former overlayer metal is a sgnificant quantity of dissociated Cd pulled into the

overlayer near-surface, again pointing up a limitation in the use of simple bulk thermodynamic data in attempting to predict complex interface behavior.

B. Schottky barrier formation

A tabulation of noble metal/CdTe Schottky barrier heights for vacuum-fabricated interfaces from other experiments[3]-[5],[22],[25]-[30] as well as ours is given in Table II, presented in the form of $E_F - E_{VBM}$. For each of the three overlayer metals, the majority of the measurements, which included the use of electrical and photoresponse techniques as well as photoemission, lie within ~0.1 eV of ours. This agreement supports the interpretation of the present results as representing the "true" Schottky barrier heights within ±0.1 eV. This will be assumed in the following discussion.

The Fermi level pinning positions for the three noble metals all fall within a narrow range of about 0.2 eV. Because the work functions ϕ_m of the noble metals span a range of 0.8 eV, with $\phi_m(Au) = 5.1$ eV and $\phi_m(Ag) = 4.3$ eV,[31] the suggested strong dependence[3]-[5],[28] of Schottky barrier height on metal work function for metals/CdTe is not supported by the present data.

The narrow range of Fermi level pinning is more consistent with defect[32] or Tersoff-type[33],[34] (MIGS) models of Schottky barrier formation. Williams *et al.*[3]-[5] and Brucker and Brillson[35] have suggested that defects such as Cd vacancies may play a role in determining the Schottky barrier height, although a calculation by Kobayashi *et al.*[36] gives a cation vacancy energy level below the VBM in CdTe. The Te_{Cd} antisite, calculated[36] to lie about 1 eV above the VBM, would be a more likely candidate for Fermi level pinning in the context of a defect model. For the Tersoff model, Tersoff's "midgap" energy lies 0.85 eV above the VBM for CdTe,[34] consistent with the Fermi level pinning observed in the present work.

C. Comparison with $Hg_{1-x}Cd_xTe$

Te dissociation and intermixing with the overlayer, discussed above for the CdTe interfaces, is very frequently observed in metal/$Hg_{1-x}Cd_xTe$ interfaces as well.[7]-[12] The extent of the Te dissociation is generally much more pronounced for $Hg_{1-x}Cd_xTe$ (MCT) than for CdTe. For instance, for Cu/MCT the Te concentration in the overlayer near-surface at high coverages is about 35%, an order of magnitude more than for Cu/CdTe.[9] The enhanced Te dissociation for MCT can be understood in terms of disruption of the MCT surface lattice due to depletion of the weakly bound Hg from the surface.

Of the three noble metals on CdTe, Ag stands out as the one for which no Cd is observed in the overlayer near-surface region. It is interesting to note that Ag also differs from the other two noble metals in its behavior on MCT. Cu/MCT (Ref. [9]) and Au/MCT (Ref. [10]) have similar interface morphologies, with at most a limited indiffusion of the overlayer metal into the semiconductor. In comparison, for Ag/MCT there is a massive motion of the overlayer metal into the semiconductor as Ag atoms replace Hg atoms in the lattice.[8] Further investigation into the causes of Cd dissociation from CdTe may conceivably also provide insight into the question of overlayer indiffusion for MCT.

VII. SUMMARY

None of the three noble metal/CdTe interfaces is entirely abrupt: all three show Te dissociation into the overlayer. For Ag and Cu, and possibly Au, the dissociated Te is in reacted form with the overlayer metal. For Cu and Au overlayers, and possibly also for Ag overlayers, the dissociated Te from the semiconductor is concentrated largely in a region within 10-20 Å of the surface of the overlayer. Dissociated Cd is observed for Cu and Au overlayers, but not for Ag overlayers. While all three overlayers may be distributed on the CdTe surface as islands for coverages below a few monolayers, for Ag overlayers clustering is observed for coverages as high as 35 Å, and possibly much higher. The Fermi level after metal deposition fell 0.8-1.0 eV above the VBM for all the interfaces studied.

ACKNOWLEDGMENTS

This work was supported by the Defense Advanced Research Projects Agency contract no. N00014-86-K-0854. Some of the crystals used in the Stanford experiments were grown at Santa Barbara Research Center.

REFERENCES

[1] L. J. Brillson, Surf. Sci. Rept. **2**, 123 (1982).

[2] K. C. Mills, *Thermodynamic Data for Inorganic Sulphides, Selenides and Tellurides* (Butterworths, London, 1974).

[3] R. H. Williams and M. H. Patterson, Appl. Phys. Lett. **40**, 484 (1982).

[4] T. P. Humphreys, M. H. Patterson, and R. H. Williams, J. Vac. Sci. Technol. **17**, 886 (1980).

[5] M. H. Patterson and R. H. Williams, J. Cryst. Growth **59**, 281 (1982).

[6] R. R. Daniels, G. Margaritondo, G. D. Davis, and N. E. Byer, Appl. Phys. Lett. **42**, 50 (1983).

[7] G. D. Davis, N. E. Byer, R. A. Riedel, and G. Margaritondo, J. Appl. Phys. **57**, 1915 (1985).

[8] D. J. Friedman, G. P. Carey, C. K. Shih, I. Lindau, W. E. Spicer, and J. A. Wilson, J. Vac. Sci. Technol. A **4**, 1977 (1986).

[9] D. J. Friedman, G. P. Carey, I. Lindau, and W. E. Spicer, Phys. Rev. B **34**, 5329 (1986).

[10] G. D. Davis, W. A. Beck, N. E. Byer, R. R. Daniels, and G. Margaritondo, J. Vac. Sci. Technol. A **2**, 546 (1984).

[11] A. Franciosi, P. Philip, and D. J. Peterman, Phys. Rev. B **32**, 8100 (1985).

[12] D. J. Friedman, G. P. Carey, I. Lindau, and W. E. Spicer, Phy Rev. B **35**, 1188 (1987).

[13] J. Chu, S. Xu, and D. Tang, Appl. Phys. Lett. **43**, 1064 (1983).

[14] W. E. Spicer, J. A. Silberman, I. Lindau, A.-B. Chen, A. Sher, and J. A. Wilson, J. Vac. Sci. Technol. A **1**, 1735 (1983).

[15] M. G. Mason, Phys. Rev. B **27**, 748 (1983).

[16] I. Lindau and W. E. Spicer, in *Synchrotron Radiation Research*, edited by H. Winick and S. Doniach (Plenum, New York, 1980).

[17] J. A. Silberman, Ph.D. thesis, Stanford University, 1986, p. 51. The VBM in these studies was located with angle-resolved photoemission at normal emission. For CdTe at photon energies near 21 eV, normal emission is much more heavily weighted by states near the VBM than is the off-normal emission detected by the CMA, permitting a more accurate determination of the VBM.

[18] J. Nogami, T. Kendelewicz, I. Lindau and W. E. Spicer, Phys. Rev. B **34**, 669 (1986).

[19] *Photoemission in Solids I*, edited by M. Cardona and L. Ley (Springer-Verlag, Berlin, 1978).

[20] P. Steiner and S. Hüfner, Acta Metall. **29**, 1885 (1981).

[21] A. R. Miedema, P. F. de Châtel, and F. R. de Boer, Physica B **100**, 1 (1980).

[22] P. John, T. Miller, T. C. Hsieh, A. P. Shapiro, A. L. Wachs, and T.-C. Chiang, Phys. Rev. B **34**, 6704 (1986).

[23] The dependence of photoelectron escape length on electron kinetic energy (Ref. [16]) shows that the escape lengths λ(Te 3d) and λ(Cd 3d) excited by Mg Kα light are nearly equal: λ(Cd 3d)/λ(Te 3d) < 1.3. This difference would not be nearly enough to explain the difference betwen the Cd 3d and Te 3d attenuations. In fact, if one assumed only clustering and no dissociation, at high coverages the Cd and Te signals would be dominated by the remaining uncovered regions of the CdTe, and the Cd and Te signals would attenuate to an equal degree.

[24] N. J. Shevchik, M. Cardona, and J. Tejeda, Phys. Rev. B **8**, 2833 (1973).

[25] T. Takebe, J. Seraie, and T. Tanaka, Phys. Status Solidi A **47**, 123 (1978).

[26] C. A. Mead and W. G. Spitzer, Phys. Rev. **134**, A713 (1964).

[27] T. F. Kuech, J. Appl. Phys. **52**, 4874 (1981).

[28] J. G. Werthen, J.-P. Häring, A. L. Fahrenbruch, and R. H. Bube, J. Appl. Phys. **54**, 5982 (1983).

[29] S. M. Sze, *Physics of Semiconductor Devices* (Wiley, New York, 1981).

[30] Williams *et al.*[3]-[5] assume the Schottky barrier height ϕ_B to be the *shift* $\Delta E_{f,s}$ in the surface Fermi level $E_{f,s}$ upon overlayer deposition. Only if the cleaved surface Fermi level $E_{f,i}$ is at the conduction band minimum (for n-type samples) will this shift be equal to $\phi_{Bn} = E_{f,s}(\text{final}) - E_{CBM}$. However, $E_{f,i}$ is often located below the CBM, as for example in the present work. The exact location of $E_{f,s}$ is widely believed to depend on the quality of the cleave. Even the bulk Fermi level may lie below the CBM depending on the sample doping. Thus it is dangerous to deduce Schottky barrier heights from $E_{f,s}$ shifts alone. For example, for Ag/n-CdTe Williams *et al.*[3]-[5] observe no $E_{f,s}$ shift and so quote $\phi_{Bn} = 0$. However, a direct examination of their photoelectron spectra[4] shows $E_{f,s}(\text{final}) - E_{VBM} \approx 1$ eV, roughly in agreement with our results. For Au/CdTe the Cd dissociation prohibits the extraction (as in Sec. III-C) of $E_{f,s}(\text{final}) - E_{VBM}$ from their spectra[4], while they appear not to have published spectra for Cu/CdTe.

[31] H. B. Michaelson, J. Appl. Phys. **48**, 4729 (1977).

[32] W. E. Spicer, I. Lindau, P. Skeath, C. Y. Su, and P. Chye, Phys. Rev. Lett. **44**, 420 (1980).

[33] J. Tersoff, Phys. Rev. B **32**, 6968 (1985).

[34] J. Tersoff, Phys. Rev. Lett. **56**, 2755 (1986).

[35] C. F. Brucker and L. J. Brillson, Thin Solid Films **93**, 67 (1982).

[36] A. Kobayashi, O. F. Sankey, and J. D. Dow, Phys. Rev. B **25**, 6367 (1982).

Table I. Heats of telluride formation ΔH_f, and heats of solution $\Delta H_{sol}(Cd;M)$ of Cd at infinite dilution in metal M, for the noble metals on CdTe.

metal (M)	telluride	ΔH_f [a] (kcal/mol)	$\Delta H_{sol}(Cd;M)$ [b] (kcal/mol)
Cd	CdTe	−24.1	
Ag	Ag_2Te	−8.6	−3.4
Cu	Cu_2Te	−10.0	−1.7
Au	$AuTe_2$	−4.5	−12.2

[a]From Ref. [2].

[b]Calculated from Miedema's semiempirical model (Ref. [21]).

Table II. Fermi level pinning positions relative to the VBM for noble metals on CdTe, from this work and other references. The corresponding Schottky barrier heights ϕ_{Bn} and ϕ_{Bp} to n- and p-type material are $\phi_{Bp} = E_F - E_{VBM}$, $\phi_{Bn} = E_g - \phi_{Bp}$.

overlayer metal	semiconductor conductivity	$E_F - E_{VBM}$ (eV)	method[a]	reference
Cu	n	1.0	P	this work
	n	1.3[d]	P	[3]
	n	1.05[b]	I	[5]
	n	1.01[b]	I,R	[25]
	p	0.9	P	this work
Ag	n	0.95	P	this work
	n	0.96	P	[22]
	n	1.0 (1.5)[d]	P	[4]
	n	>1.2[b]	C	[4]
	n	0.69[b,c]	C	[26]
	n	0.84[b]	R	[26]
Au	n	0.65[d]	P	[4]
	n	0.79[b,c]	C	[26]
	n	0.54[b]	C	[4]
	n	0.81[b]	C	[25]
	n	0.90[b]	I	[26]
	n	0.85[b]	I,C,R	[27]
	n	0.90[b]	I,R	[25]
	p	0.8	P	this work
	p	0.65	I,C	[28]

[a]P: Photoemission; I: I-V electrical; C: C-V electrical; R: photoResponse.

[b]Calculated from $E_F - E_{VBM} = E_g - \phi_{Bn}$, with $E_g = 1.50$ eV.

[c]Quoted by Sze (Ref. [29]).

[d]See comments in Ref. [30].

FIGURE CAPTIONS

1. (a) He I ($h\nu$=21.2 eV) spectra of the valence band with increasing coverage of Au on CdTe.
   (b) Comparison of the He I valence band spectrum of 17 ML Au/CdTe with an Au/stainless steel reference spectrum.
2. He I ($h\nu$=21.2 eV) spectra of the Cd 4d shallow core levels with increasing coverage of Au on CdTe. Energies are referred to E_F.
3. (a) Attenuation (natural log scale) of the XPS peak areas I of the CdTe core levels with increasing Au coverage. The peak areas are normalized to their zero-coverage values I_0.
   (b) The intensity ratio $R(\Theta)\equiv I_{Te\ 3d}(\Theta)/I_{Te\ 4d}(\Theta)$ normalized to the zero-coverage value R(0), for Au/CdTe.
4. Variation of the Te 3d and Au 4f core widths (FWHM) with coverage for Au/CdTe. The widths are normalized to the 0 ML coverage for the Te 3d core level, and to the 0.1 ML coverage for the Au 4f core level.
5. Comparison of the kinetic energy shifts of the Cd 4d ($h\nu$=40.8 eV) and Cd 3d ($h\nu$=1253.6 eV) centroids as a function of Au coverage. The shifts are defined to be zero at Θ=0 ML for both the 4d and 3d core levels, as indicated by the superposed filled diamond (Cd 3d) and unfilled diamond (Cd 4d) symbols at Θ=0 ML. Note the shift of ~0.15 eV to lower kinetic energy between Θ=0 ML and Θ=0.1 ML for both core levels.
6. He I ($h\nu$=21.2 eV) spectra of the valence band with increasing coverage of Ag on CdTe.
7. He I ($h\nu$=21.2 eV) spectra of the Cd 4d shallow core levels with increasing coverage of Ag on CdTe. Energies are referred to E_F.
8. Attenuation (natural log scale) of the XPS peak areas I of the CdTe core levels with increasing Ag coverage. The peak areas are normalized to their zero-coverage values I_0.

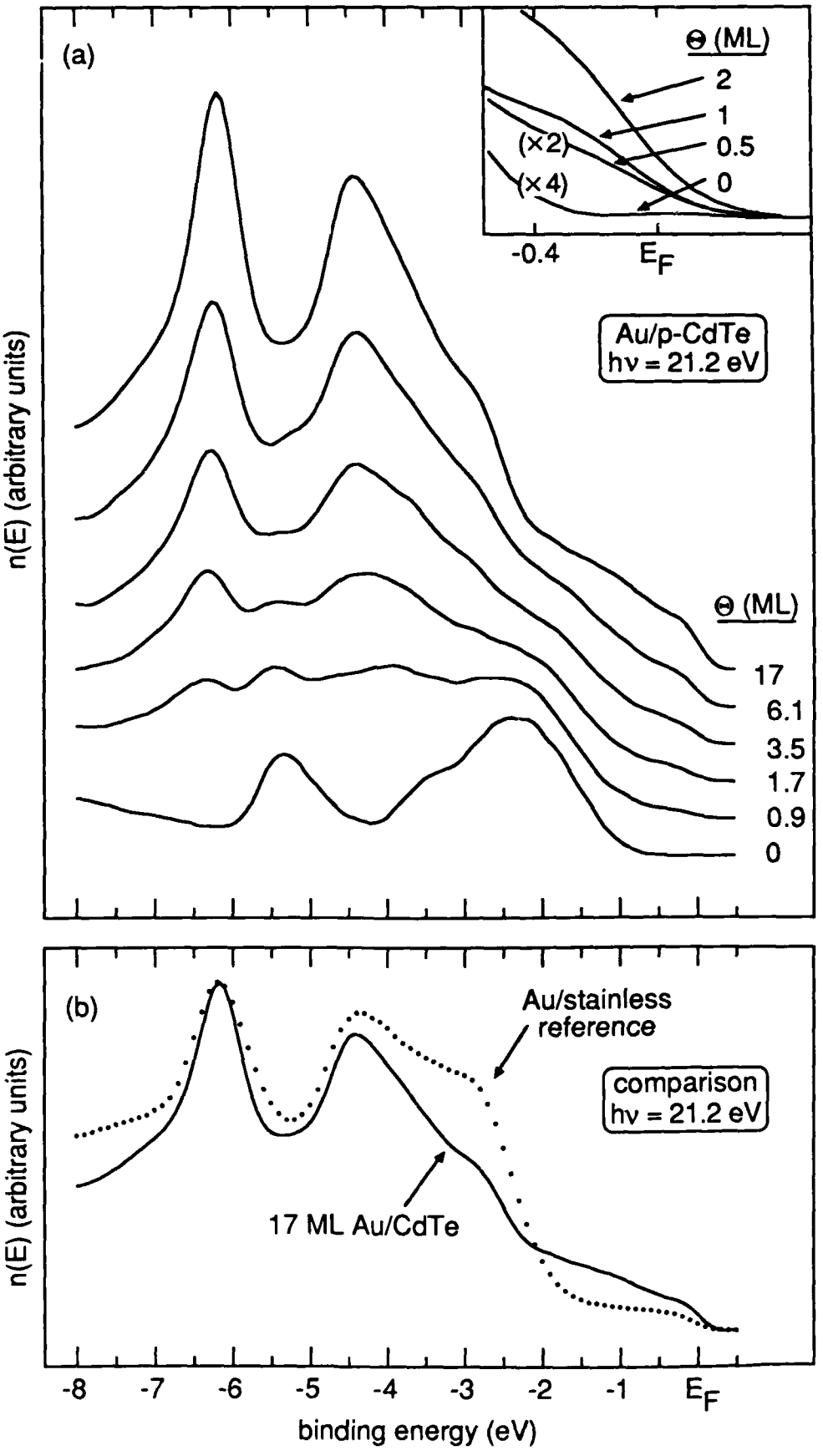
(a)
Θ (ML)
2
1
0.5
0
(×2)
(×4)
-0.4
E_F
Au/p-CdTe
hν = 21.2 eV
n(E) (arbitrary units)
Θ (ML)
17
6.1
3.5
1.7
0.9
0
(b)
Au/stainless
reference
comparison
hν = 21.2 eV
17 ML Au/CdTe
n(E) (arbitrary units)
-8
-7
-6
-5
-4
-3
-2
-1
E_F
binding energy (eV)

Figure 1

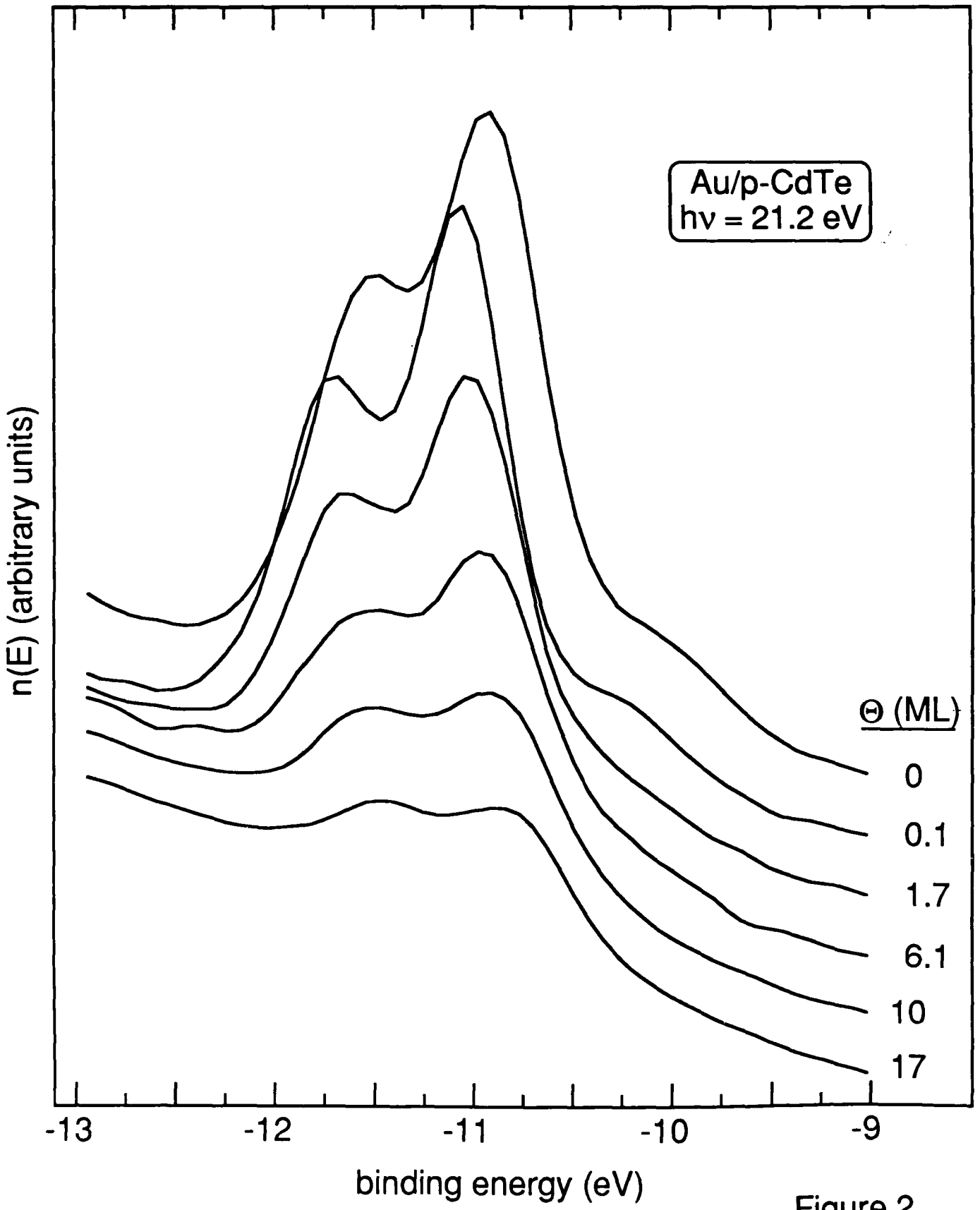
Au/p-CdTe
hν = 21.2 eV
Θ (ML)
0
0.1
1.7
6.1
10
17
n(E) (arbitrary units)
-13
-12
-11
-10
-9
binding energy (eV)

Figure 2

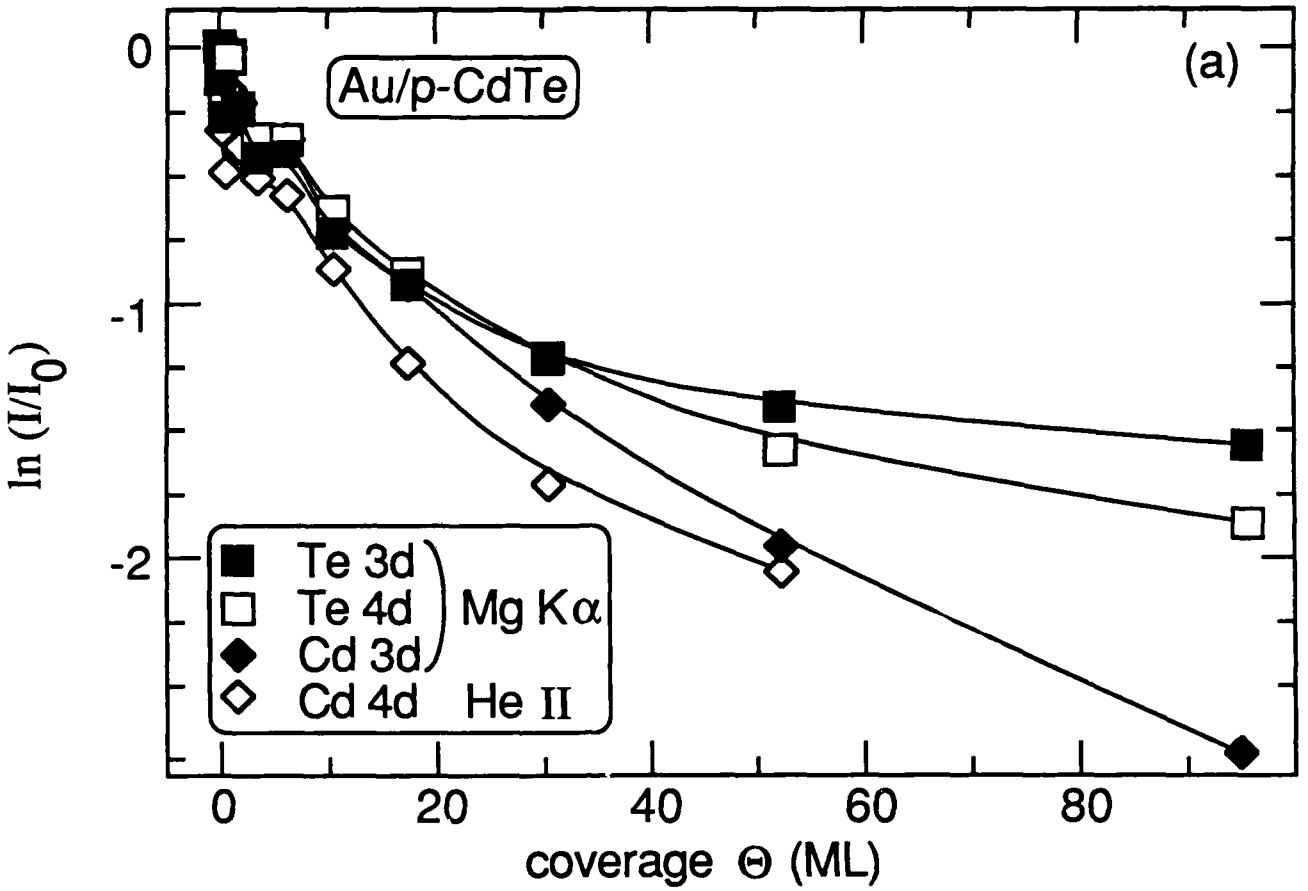
Au/p-CdTe
(a)
0
-1
-2
ln (I/I0)
Te 3d
Te 4d
Cd 3d
Cd 4d
Mg Kα
He II
0
20
40
60
80
coverage Θ (ML)

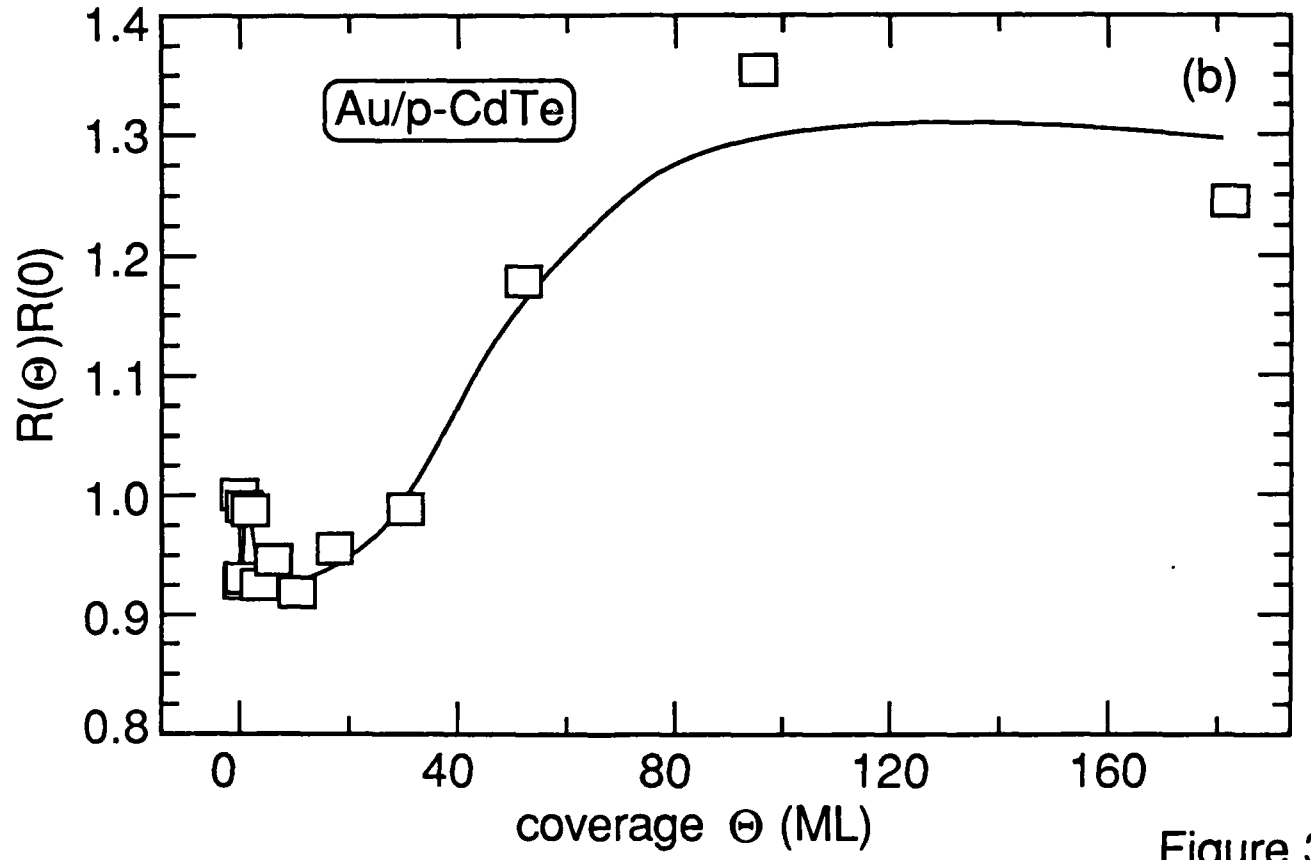
Au/p-CdTe
(b)
1.4
1.3
1.2
1.1
1.0
0.9
0.8
R(Θ)R(0)
0
40
80
120
160
coverage Θ (ML)

Figure 3

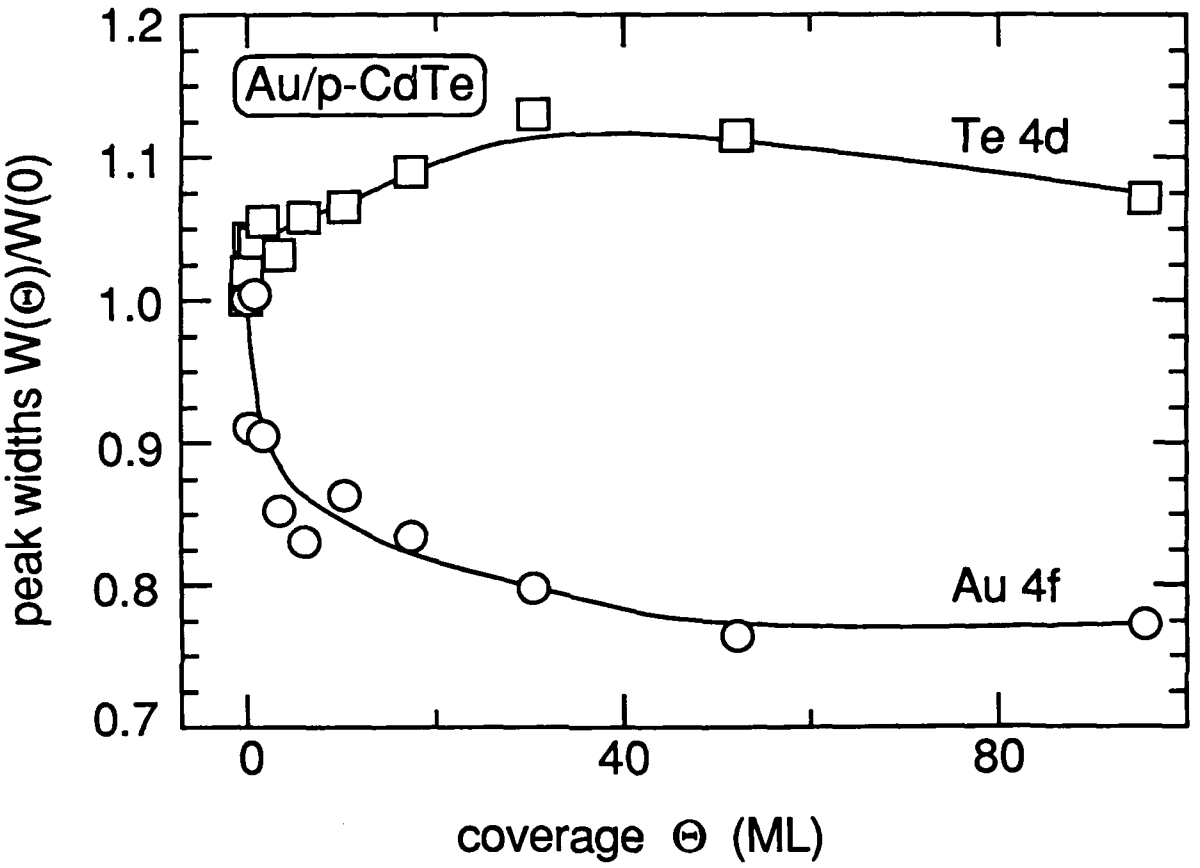
Au/p-CdTe
Te 4d
Au 4f
peak widths W(Θ)/W(0)
coverage Θ (ML)
1.2
1.1
1.0
0.9
0.8
0.7
0
40
80

Figure 4

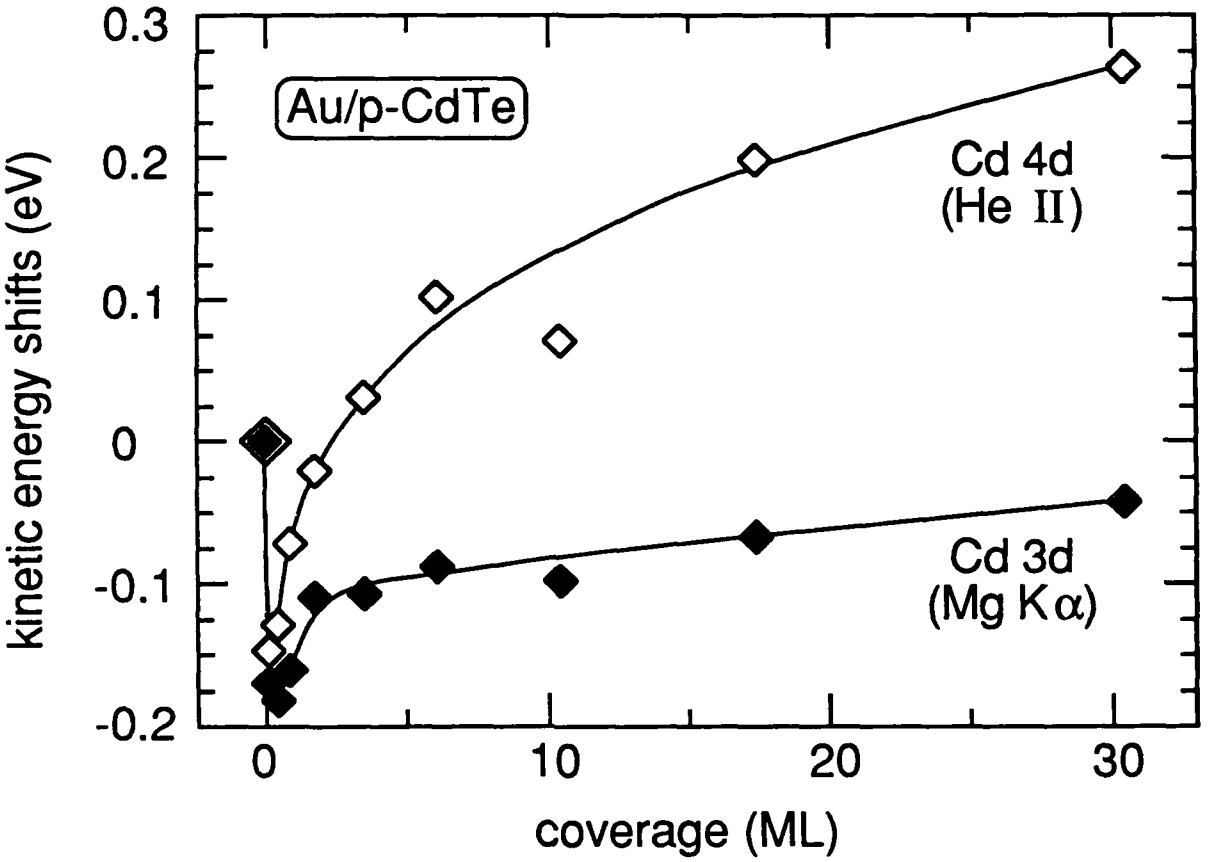
Au/p-CdTe
Cd 4d
(He II)
Cd 3d
(Mg Kα)
kinetic energy shifts (eV)
coverage (ML)
0.3
0.2
0.1
0
-0.1
-0.2
0
10
20
30

Figure 5

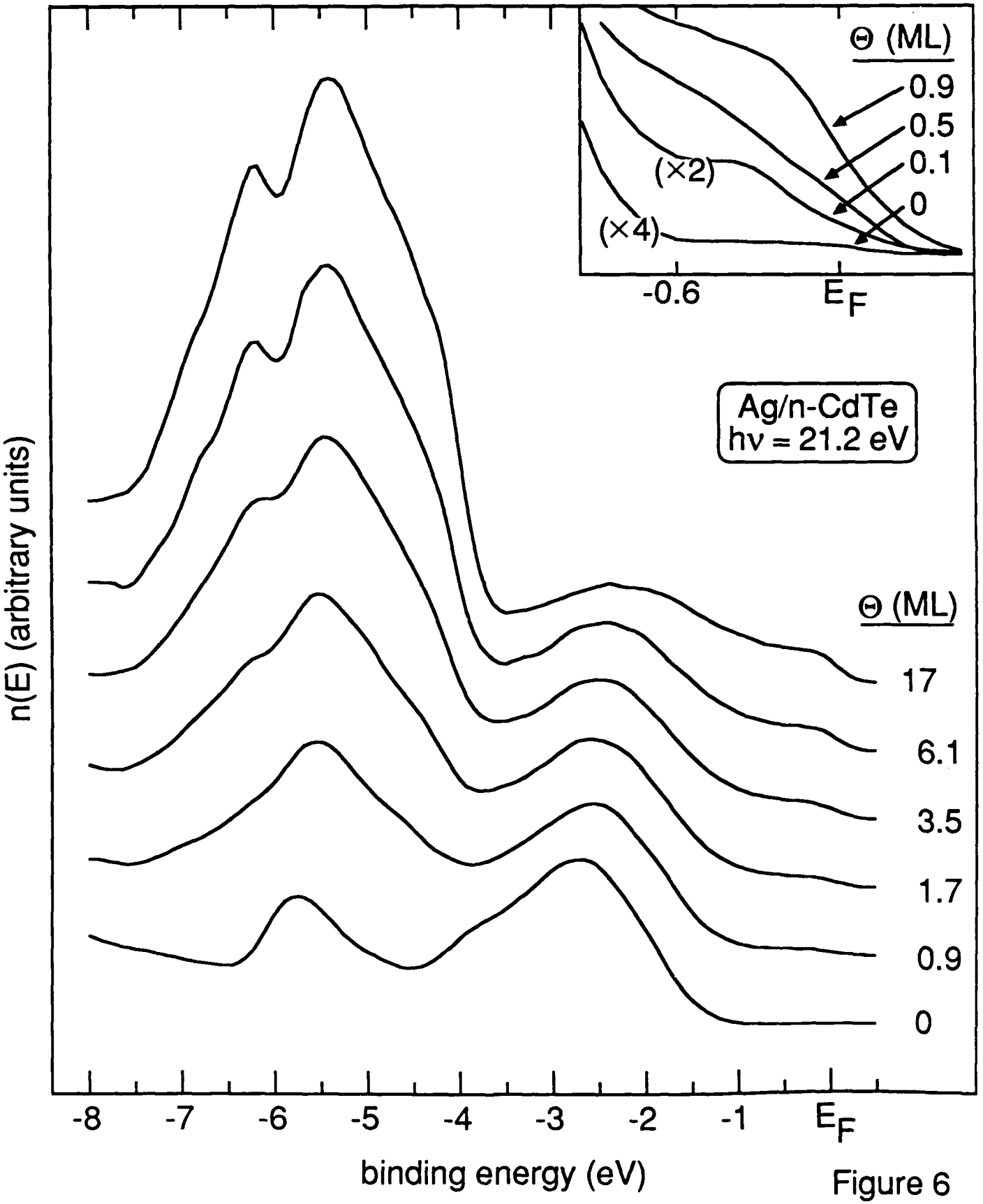
Θ (ML)
0.9
0.5
0.1
0
(×2)
(×4)
-0.6
E_F
Ag/n-CdTe
hν = 21.2 eV
Θ (ML)
17
6.1
3.5
1.7
0.9
0
n(E) (arbitrary units)
-8
-7
-6
-5
-4
-3
-2
-1
E_F
binding energy (eV)

Figure 6

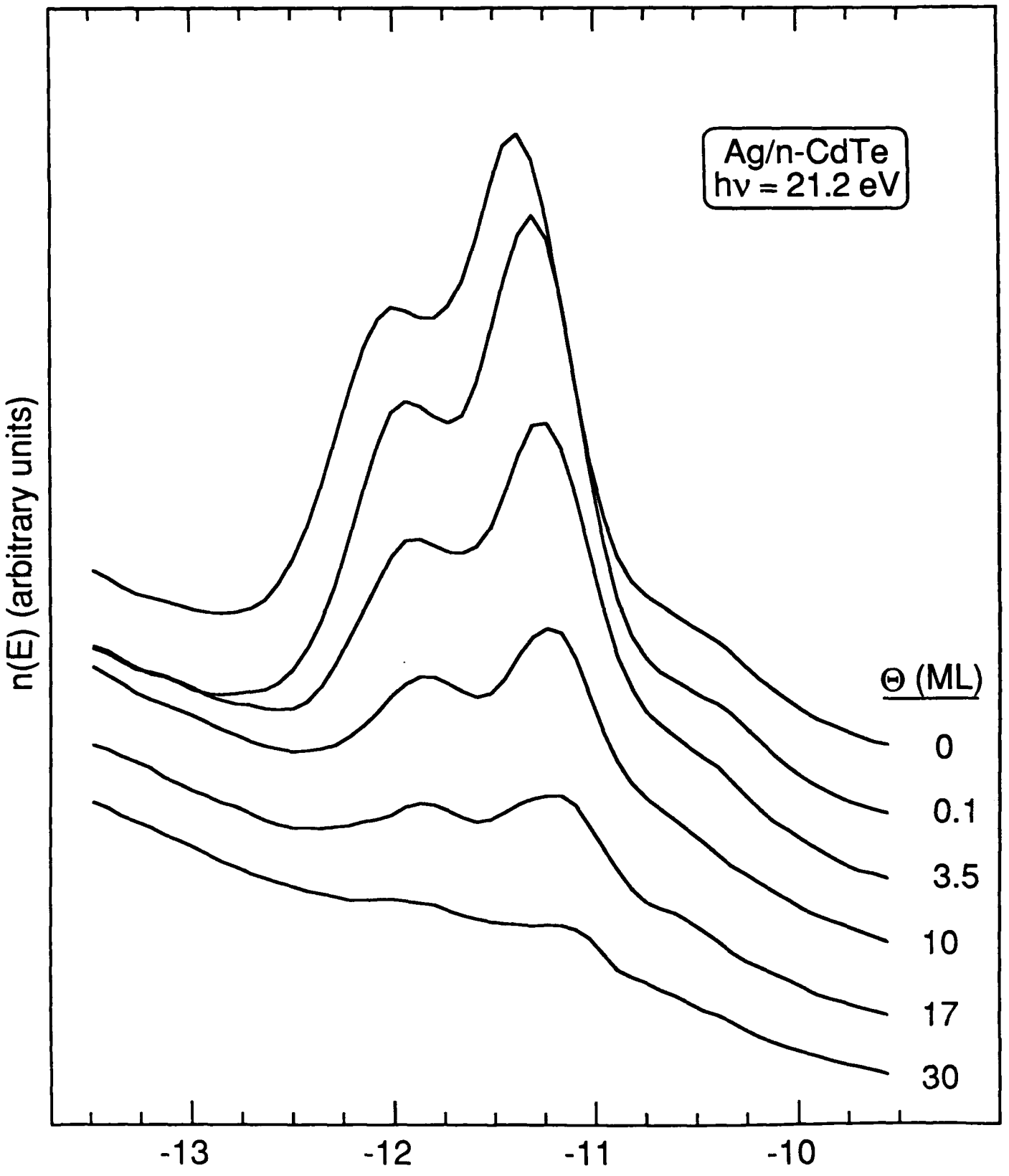
Ag/n-CdTe
hν = 21.2 eV
n(E) (arbitrary units)
Θ (ML)
0
0.1
3.5
10
17
30
-13
-12
-11
-10
binding energy (eV)

Figure 7

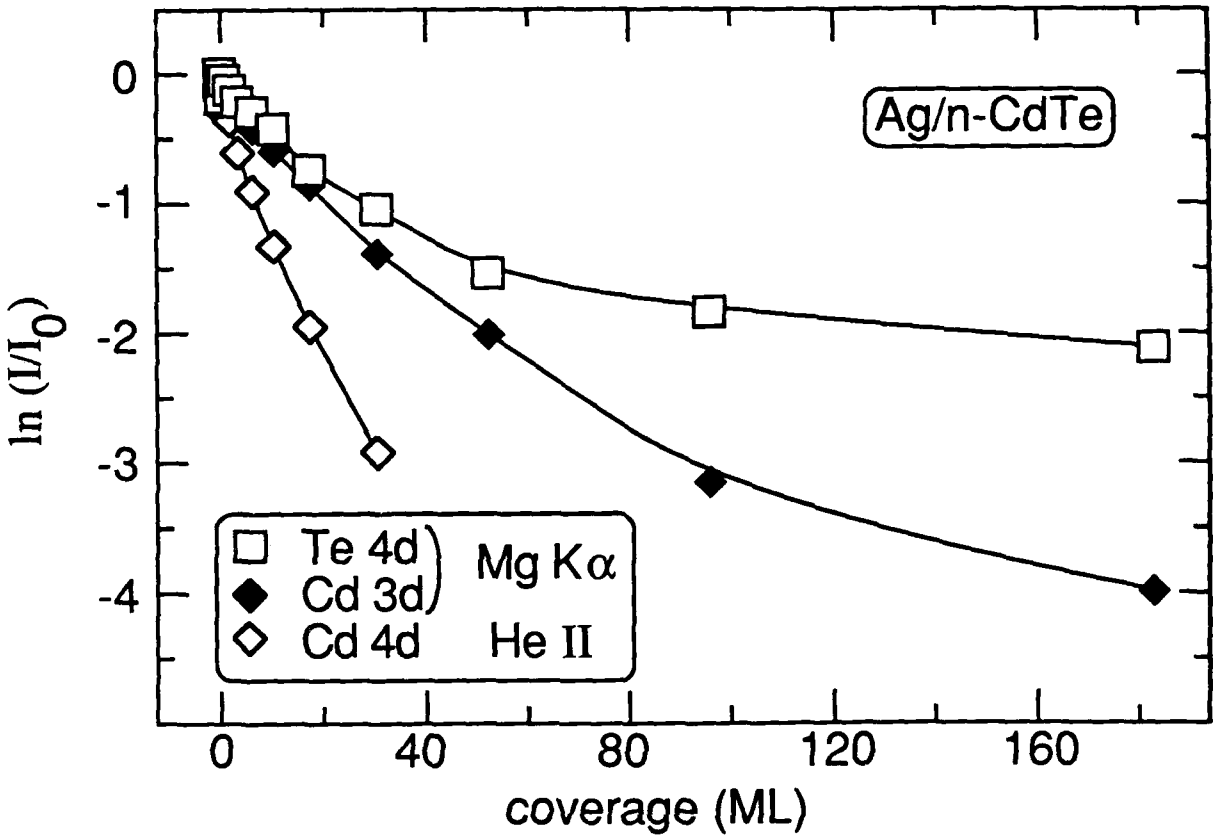
Ag/n-CdTe
0
-1
-2
-3
-4
ln (I/I0)
Te 4d
Cd 3d
Cd 4d
Mg Kα
He II
0
40
80
120
160
coverage (ML)

Figure 8